Incorporating hydrothermal liquefaction into wastewater treatment – Part I: Process optimization for energy recovery and evaluation of product distribution

Huan Liu, Ibrahim Alper Basar, Nathalie Lyczko, Ange Nzihou, Cigdem Eskicioglu

Incorporating hydrothermal liquefaction into wastewater treatment – Part I: Process optimization for energy recovery and evaluation of product distribution

Huan Liu [a], Ibrahim Alper Basar [a], Nathalie Lyczko [b], Ange Nzihou [b,c,d], Cigdem Eskicioglu [a,*]

[a] UBC Bioreactor Technology Group, School of Engineering, The University of British Columbia, Okanagan Campus, 1137 Alumni Avenue, Kelowna, British Columbia V1V 1V7, Canada
[b] Université de Toulouse, IMT Mines Albi, RAPSODEE CNRS UMR 5302, Campus Jarlard, F.81013 Albi Cedex 09, France
[c] Princeton University, School of Engineering and Applied Science, Princeton, NJ 08544, USA
[d] Princeton University, Andlinger Center for Energy and the Environment, Princeton, NJ 08544, USA

A B S T R A C T

The treatment of significant amounts of municipal sewage sludge requires novel and efficient technologies. This study evaluated hydrothermal liquefaction as a means to sustainably convert sludge waste into a renewable energy source – biocrude, which can mitigate both environmental and energy-related challenges. Response surface methodology was employed to investigate the effects of reaction temperature (290–360 °C) and residence time (0–30 min) on product yield and biocrude quality. Both the highest and the lowest reaction temperature or residence time had negative effects on biocrude yield and energy recovery (ER), while high reaction severities improved biocrude quality. Under optimized conditions (332 °C for 16.9 min), biocrude yield (48.9%, dry ash-free) and ER (70.8%) were maximized. Biocrude composition followed the order of N-heterocycles > O-heterocycles > hydrocarbons, while nitrogenous compounds reduced, and hydrocarbons increased with reaction temperature. More distillable fractions in biocrude were also produced at higher reaction severities. The possible reaction pathways of biocrude formation were discussed and updated to include catalytic effects on inherent metals and Brønsted (acidic and basic) sites. The high content of O (7.8–13.1%), N (4.4–4.9%), and TAN (48.6–63.6 mg KOH/g) suggested the necessity of biocrude upgrading. Separating and recycling trace metals (e.g., 497–656 mg/kg Fe) from biocrude are necessary to relieve upgrading challenges. C, N, and P were mostly distributed into HTL biocrude, aqueous, and hydrochar, respectively, allowing their recovery. Most metals were concentrated in hydrochar. The results contribute to the advancement of the state of the art in biorefinery, which will guide the design of full-scale HTL sludge treatment systems combining resource recovery.

1. Introduction

With increasing population and rapid urbanization, municipal wastewater treatment plants (WWTPs) generate a significant amount of wastewater solids (often called municipal sludge or sewage sludge), which require further treatment and disposal. Canada and the US reported an annual sludge production of >660000 dry tonnes (approximately 2.5 million wet tonnes) and 12.7 million dry tonnes (approximately 56 million wet tonnes), respectively [1,2]. The known total sludge production rate from medium- and high-income countries was reported as 40 million dry tonnes per year [3]. Moreover, such a large amount is expected to keep rising due to population growth and increasingly stringent requirements for wastewater treatment. The current strategy of sludge disposal includes land application, incineration, and landfilling. More than half of total sludge in Canada is land applied after being stabilized (i.e., biosolids). The biological stabilization techniques (e.g., anaerobic digestion and composting) require a long sludge retention time (over 15 days), which are cost ineffective. Additionally, land application of biosolids is vulnerable to market fluctuations, such as high costs of transportation, agricultural land being saturated with nutrients, and public opposition due to the presence of pathogens and contaminants (e.g., hormones, pesticides, and heavy metals) [4].

* Corresponding author.
E-mail addresses: liu@alumni.ubc.ca (H. Liu), alperbasar@alumni.ubc.ca (I.A. Basar), lyczko@mines-albi.fr (N. Lyczko), ange.nzihou@mines-albi.fr (A. Nzihou),

Incinerating sludge requires significant expenditures and energy inputs [5]. Landfilling sludge is restricted for over-generating methane and wasting organic matters and nutrients [6]. Considering the growing sludge production and climate change concerns, alternate options for sustainable sludge treatment, such as waste-to-energy conversion, are demanded and have attracted extensive research.

Due to the high moisture content (almost 98%, by weight) and massive volume of raw sludge, its handling is challenging and costly. A novel technique, hydrothermal liquefaction (HTL), is considered one of the most promising technologies to address those challenges environmentally friendly, efficiently, and economically [7]. Municipal sludge is often seen as waste, but HTL converts sludge into biocrude that can be refined to a low-carbon fuel. HTL does not require drying processes but instead uses hot pressurized water as a reaction medium through a thermochemical process. This ability significantly reduces the energy input compared to other techniques that require dry feedstocks (e.g., incineration and pyrolysis) [8]. HTL can also efficiently decompose organic matter/pollutants and reduce the volume of residual solids by using elevated temperature (280–374 °C) and pressure (8–22 MPa) in a short period (typically < 30 min) [9]. After HTL, maximum C is converted into biocrude while most P is enriched in hydrochar to allow its recovery, representing a justifiable and sustainable operation for sludge treatment. Several studies also suggested that hydrothermal treatment especially HTL can remove most micropollutants [10–12]. In summary, HTL can be simultaneously used for waste-to-energy conversion, organic pollutants destruction, waste minimization, and sterilization for final disposal.

A successful bench-scale continuous-flow test at the Pacific Northwest National Laboratory (PNNL) has demonstrated that HTL is capable of handling municipal sludge, and the subsequent hydrotreating turned biocrude into liquid fuel [2]. A significant reduction (94–99%) of residual solids for disposal was also achieved. Such success shows a way to beneficially utilize waste and produce biofuel from clean and renewable resources, which addresses the global demand for low carbon energy. Currently, Metro Vancouver in British Columbia (BC, Canada) is leading the design of a pilot-scale HTL demonstration unit at the Annacis Island WWTP. However, several extensive literature reviews [3,13,14] identified many research gaps that need to be addressed before an HTL system can be successfully incorporated into a WWTP. First and foremost, the operational conditions of the HTL system need to be optimized for energy recovery and economically sustainable operation. The optimum HTL conditions are usually feedstock-specific due to the difference in biochemical compositions. Using model compounds, it has been identified that energy recovery (ER) in biocrude from HTL (350 °C) of different feedstocks followed the order of lipids (82.7–86.7%) > proteins (10.7–36.4%) > carbohydrates (8.3–13.7%) > lignin (2.5%) [15,16]. Synergistic effects on biocrude yield and ER were also found from binary mixtures of proteins–carbohydrates, proteins–lipids, and carbohydrates–lignin due to the Maillard reaction, amides formation, and potential *retro*-aldol reactions favored by alkaline lignin, respectively [16,17]. Therefore, using a feedstock balanced with various biochemical compounds can take advantage of those synergies for maximizing biocrude production and ER. In a typical WWTP, primary and secondary sludges are generated, which are rich in carbonates/lipids and protein, respectively [14]. Their mixture (mixed sludge) represents a balanced feedstock for HTL. On the other hand, the improvement by those synergies also depends on specific compositions of feedstock and HTL operational conditions [17,18]. Therefore, process optimization is crucial for implementing HTL to a typical WWTP.

To date, only two studies used the response surface methodology (RSM) to optimize the conditions for HTL of primary sludge and co-HTL of waste activated sludge and sawdust regarding biocrude yield [19,20]. To the best of the authors' knowledge, optimization of HTL parameters aiming for biocrude ER from mixed sludge was never evaluated. This study was motivated to address the research gap and provide guidance in designing a pilot and subsequently a full-scale WWTP incorporating HTL sludge treatment. HTL reaction temperature and residence time have shown dominant effects on HTL products [13,14], and thus they were investigated in this study. As RSM can effectively optimize experimental conditions with a minimum number of experimental runs, it was used to design the HTL batch experiments. Multiple response models were developed using RSM: Yield of HTL products (biocrude, hydrochar, aqueous, and gas) and biocrude quality parameters, such as carbon recovery (CR), higher heating value (HHV), energy recovery (ER), energy return on investment (EROI), and total acid number (TAN). The optimization results for maximized biocrude ER were validated with additional experiments. Besides, the effects of experimental factors on biocrude characteristics were investigated. Finally, the elemental distribution among HTL products was presented to guide their proper utilization.

2. Materials and methods

2.1. Materials

Considering the common process configuration of primary and secondary treatment in WWTPs, mixed primary and secondary sludge was selected as the HTL feedstock for the baseline model. Thickened screened primary sludge (TSPS) and thickened waste secondary sludge (TWSS) were collected from Annacis Island WWTP in Delta, BC, Canada. Once received, TSPS and TWSS were mixed in a volume ratio of 1:1 based on the average annual flow, also representative of a typical plant. The mixed sludge was dewatered to 20 wt% total solids (TS) content by centrifugation and stored at 4 °C before experiments. A portion of mixed sludge was dried at 105 °C for 24 h and pulverized to pass No. 60 (250 μm) sieve for characterization. Anhydrous dichloromethane (DCM, ≥99.8%) was purchased from Sigma-Aldrich and used for reactor rinsing/washing and biocrude extraction. Type I water with a resistivity of 18.2 MΩ cm @ 23 °C was used for all reagent preparation.

2.2. Bench-scale HTL experiments

All HTL batch experiments were conducted on dewatered mixed sludge (20 wt% TS) in a bench-top pressure reactor (Parr® 4570). The reaction cylinder was made of Alloy C-276 with an inside volume of 1 L, with an inner diameter of 9.525 cm and a depth of 15.748 cm. To achieve a fast-heating rate, the cylinder was equipped with two heaters: A shell heater surrounding the cylinder and a band heater assigned to the cylinder head, controlled by Parr® 4848 Controller and Parr® 4838 Controller, respectively. In each experiment, the reaction cylinder was loaded with 500.0 ± 0.1 g of sludge sample and sealed. Nitrogen gas was purged through the gas inlet for 5 min to create an inert environment in the vessel. As fast heating or short ramping time has been found beneficial to biocrude yield [21–23], the reactor was heated at the fastest heating rate from room temperature (22–23 °C) to the desired reaction temperature (290–360 °C) in approximately 1 h. Continuous agitation of 500 rpm was employed throughout the reaction by a magnetic drive. Once the reactor reached the reaction temperature, it was held for the desired residence time (0–30 min). Thereafter, the reactor was turned off and the vessel was cooled to room temperature in 1–2 h by running cold water through the internal cooling coil. The temperature profiles were shown in the supplementary material (Fig. S1).

2.3. HTL products separation

After the reactor cooled to room temperature, the gas produced during HTL was collected in a 10-L Tedlar bag for the determination of volume and compositions. The reactor was opened and the mixture of HTL aqueous, biocrude, and hydrochar were collected and centrifuged at 4000 × g for 15 min. The water-soluble supernatant was filtered using a pre-weighed hydrophilic nylon membrane (20 μm pore size) and the filtrate was collected and referred to as HTL aqueous phase. The

remained biocrude and hydrochar mixture (centrifugation cake and filtration residue) was washed with approximately 1 L dichloromethane (DCM) and filtered with the pre-weighed membrane. The filtered cake was transferred into 50 mL centrifuge tubes, extracted with DCM by vortex at 3,000 rpm for 30 s [23]. After centrifuging at 10000 × g for 10 min, the DCM-soluble phase was filtered (20 μm nylon membrane) and collected. The extraction was repeated until the filtrate became colorless. The DCM-insoluble solid residue was referred to as hydrochar. The filtrate was evaporated at 45 °C for approximately 2 h under reduced pressure to remove DCM using a rotary evaporator and the remaining black viscous liquid was donated as biocrude.

2.4. Experimental design

A circumscribed central composite (CCC) design was used in the RSM to arrange experiments, which allows for the exploration of factorial effects on response beyond or below the chosen variable range by examining outer extreme axial points. As shown in Table 1, the design included two variables and five levels with a total of 19 runs. It consists of 4 factorial points (coded as ± 1) in duplicate, 4 axial points (coded as ± 1.41) in duplicate, and a triplicate of the center point (coded as 0). A polynomial regression model expressed by Eq. (1) was performed to examine the interactive relationships between the variables and the responses. The analysis of variance (ANOVA) was used to analyze the experimental data and evaluate the statistical significance of the model at a confidence level of 95% using Design-Expert® Version 13.

$$Y_r = \beta_0 + \sum_{i=1}^{3}\beta_i X_i + \sum_{i=1}^{3}\beta_{ii}X_i^2 + \sum_{i=1}^{2}\sum_{j>i}^{3}\beta_{ij}X_iX_j \quad (1)$$

Where Y_r is the response variable; X_i and X_j are the independent variables; β_0, β_i, β_{ii}, and β_{ij} are the intercept, linear, quadratic, and interaction coefficients of the model, respectively.

2.5. HTL product yields and energy recovery

Samples of dewatered sludge feedstock and hydrochar were dried in an oven at 105 °C for 24 h to measure dry matter content. The volume of produced gas was measured using a gas flow meter (Alicat M−series, accuracy ± 0.6%) in an air-conditioned room, and the mass was calculated using the ideal gas law by Eqs. (2) and (3). To minimize the systematic error for calculations, the ambient pressure and temperature were recorded during the measurement using a digital pressure gauge (Keller LEO2, accuracy ± 0.1%) and digital hygrometer (ThermoPro TP49, accuracy ± 1 °C), respectively. The error for gas mole number (n) was estimated within 0.7%.

$$n = \frac{PV}{RT} \quad (2)$$

$$m = nM \quad (3)$$

where
n = mole number of HTL gas (mol);
P = pressure of HTL gas (atm);
V = volume of HTL gas (L);
R = ideal gas constant (0.08205 L atm/mol K);
T = absolute temperature of HTL gas (K);
m = mass of HTL gas (g); and,
M = average molar mass of HTL gas (g/mol).

The yields (Y) on a dry basis (db) and dry ash-free basis (daf) of biocrude, hydrochar, and HTL gas were calculated by Eqs. (4) and (5), respectively, while the difference was attributed to HTL aqueous.

$$Y(\%, db) = (dry\ mass\ of\ product / dry\ mass\ of\ sludge\ feedstock) \times 100 \quad (4)$$

$$Y(\%, daf) = (dry\ ash\ free\ mass\ of\ product / dry\ ash\ free\ mass\ of\ sludge\ feedstock) \times 100 \quad (5)$$

ER and EROI were calculated based on Eqs. (6) to (9) [24,25]:

$$ER(\%) = Y_{product} \times HHV_{product} / HHV_{feedstock} \quad (6)$$

Table 1
Independent variables and levels (code) of CCC design for HTL experiments and product yield.

Run	Factors		Yield (%, db)[a]				Yield (%, daf)[a]			
	Reaction temperature (°C)	Residence time (min)	Biocrude	Hydrochar	Aqueous	Gas	Biocrude	Hydrochar	Aqueous	Gas
1	325 (0)	15 (0)	43.2	15.1	33.0	8.8	48.1	6.4	35.7	9.8
2	350 (1)	25.6 (1)	41.0	13.8	35.2	10.1	45.6	4.9	38.2	11.3
3	300 (–1)	25.6 (1)	40.1	17.4	34.4	8.1	44.8	8.9	37.3	9.1
4	300 (–1)	25.6 (1)	41.2	15.6	34.8	8.4	45.9	7.0	37.7	9.4
5	350 (1)	4.4 (–1)	41.4	13.5	36.3	8.8	46.2	4.7	39.3	9.8
6	300 (–1)	4.4 (–1)	36.5	17.6	39.7	6.2	40.7	10.2	42.2	6.9
7	325 (0)	15 (0)	43.4	15.1	33.4	8.2	48.4	6.4	36.2	9.1
8	350 (1)	25.6 (1)	40.2	13.6	36.1	10.1	44.9	4.7	39.1	11.3
9	300 (–1)	4.4 (–1)	36.9	17.0	39.5	6.6	41.2	9.6	41.8	7.4
10	350 (1)	4.4 (–1)	41.9	13.9	35.7	8.5	46.7	5.4	38.5	9.5
11	360 (1.41)	15 (0)	40.6	15.1	34.6	9.8	45.2	5.9	37.9	10.9
12	290 (–1.41)	15 (0)	38.9	17.2	36.5	7.5	43.3	9.3	38.9	8.4
13	325 (0)	0 (–1.41)	38.8	16.9	36.7	7.6	43.3	7.8	40.3	8.5
14	325 (0)	15 (0)	42.8	15.6	33.1	8.5	47.7	6.6	36.2	9.5
15	360 (1.41)	15 (0)	41.3	14.3	34.4	10.1	46.1	5.4	37.3	11.3
16	290 (–1.41)	15 (0)	37.5	16.5	38.5	7.6	41.8	8.4	41.4	8.5
17	325 (0)	0 (–1.41)	39.9	16.6	35.9	7.6	44.6	7.6	39.4	8.5
18	325 (0)	30 (1.41)	40.3	15.6	34.9	9.2	44.9	6.3	38.5	10.3
19	325 (0)	30 (1.41)	40.8	15.5	34.7	9.0	45.5	6.4	38.1	10.0

[a] db = dry basis; daf = dry ash-free.

$$EROI = energy\ output/energy\ input \quad (7)$$

$$Energy\ output = HHV_{biocrude} \times m_{biocrude} \quad (8)$$

$$Energy\ input = m_F \times C_P \times (T - T_0) \quad (9)$$

where

HHV = higher heating value (MJ/kg);

$m_{biocrude}$ = total mass of produced biocrude (kg);

m_F = mass of sludge feedstock (kg);

C_P = specific heat capacity of municipal sludge (equivalent to water, 4.186×10^{-3} MJ/kg °C);

T = HTL reaction temperature (°C); and,

T_0 = room temperature (23 °C).

2.6. Characterization of sludge feedstock and HTL products

Ash contents in dried dewatered sludge and hydrochar were measured by burning at 750 °C for 2 h following the American Society for Testing and Materials (ASTM) Method D3174–12. Ash content of biocrude was determined by burning at 750 °C until all carbonaceous material disappeared according to the ASTM D482–19. Ultimate analyses (C, H, N, and S) were conducted by an automatic elemental analyzer (Costech ECS 4010). The content of O was estimated by the difference of C, H, N, S, and ash. The main components (N_2, O_2, CO_2, and CH_4) of HTL gases were analyzed using an Agilent 7820A gas chromatography with a thermal conductivity detector (GC-TCD) equipped with a packed column (Agilent G3591-8003/80002). The pH of sludge was determined using a pH meter (Fisher Accumet Model 320). The TAN in biocrude was measured by the color-indicator titration method (ASTM D974–14). The HHV of dried sludge and biocrude were determined by a bomb calorimeter (IKA C5000). The inorganic elements were extracted by microwave-assisted acid digestion following the US Environmental Protection Agency (EPA) Method 3051A. All extracts were diluted to 1% (v/v) nitric acid concentration and analyzed by an Agilent 8900 Triple Quad inductively coupled plasma mass spectrometry (ICP-MS). The characteristics of mixed sludge were presented in Tables 2 and 3.

Thermogravimetry and differential scanning calorimetry (TGA-DSC) analysis was performed on biocrude using a TA Instruments SDT Q600 analyzer. Approximately 10 mg of sample was heated at a heating rate of 2 °C/min from 30 to 700 °C with a nitrogen (N_2) or air purge rate of 100 mL/min. Results were obtained by subtracting blank measurements with the empty platinum crucible.

Gas chromatography-mass spectroscopy (GC–MS) analysis of biocrude was performed using a GCMS-TQ8030 (Shimadzu, Japan) equipped with a capillary column (RXi-5SiMS, 30 m × 0.25 mm × 0.25 μm). Isopropanol was the solvent and the carrier gas (helium) was used at a flow rate of 3 mL/min. The column temperature was programed as follows: Hold at 50 °C for 5 min, ramp to 180 °C at a heating rate of 4 °C/min, ramp to 280 °C at a heating rate of 16 °C/min, and hold at 280 °C for 5 min. The temperatures of injection, ion source, and interface were set at 250, 250, and 260 °C, respectively. Samples were injected with a split ratio of 1:10. Full-scan mass spectra were performed at a mass range of 40–600 m/z in Q3 scan mode after a 2.5 min solvent delay. The mass spectra libraries of NIST11 and NIST11s were used to identify compounds. The relative area percentages of identified peaks were calculated by integrating the total ion chromatogram (TIC). Detailed information was included in Table S1.

Table 2
Proximate and ultimate analyses of dewatered mixed sludge.

Parameter[a]	Values (n = 2)
pH	5.97 ± 0.04
Alkalinity (mg $CaCO_3$/L)	2433.0 ± 0.0
Volatile fatty acids (mg/L)	746 ± 35
Volatile matter (%, db)	78.6 ± 0.5
Ash (%, db)	10.5 ± 0.1
Fixed carbon (%, db)	10.9 ± 0.5
C (%, db)	47.6 ± 0.1
H (%, db)	6.8 ± 0.1
N (%, db)	5.4 ± 0.1
S (%, db)	0.9 ± 0.0
O (%, db)	28.8 ± 0.1
HHV (MJ/kg, db)	22.1 ± 0.1

[a] db – dry basis.

Table 3
Metal species in dewatered mixed sludge (n = 3).

Inorganics	Concentration (mg/kg, dry basis)
Alkali metals	
Na	359 ± 75
K	1395 ± 122
Alkaline earth metals	
Ba	1001 ± 6
Ca	6915 ± 797
Mg	2370 ± 113
Transition metals	
Cd	<0.06
Cr	26.9 ± 0.5
Co	1.72 ± 0.02
Cu	230 ± 9
Fe	9819 ± 375
Mn	112 ± 1
Mo	6 ± 1
Hg	0.8 ± 0.1
Ni	11.4 ± 0.5
Ag	1.6 ± 0.1
V	4.2 ± 0.1
Zn	548 ± 9
Post-transition metals	
Al	2691 ± 136
Pb	17 ± 2
Non-metals	
As	1.8 ± 0.2
Se	2.4 ± 0.6
P	13909 ± 74

3. Results and discussion

3.1. Product yields and modeling

Response surface methodology was applied to investigate the effect of experimental variables on product yields. Dry ash-free yields were used as the responses to obtain better models that are applicable to various sludge feedstock. The yields (Y) of biocrude, hydrochar, aqueous, and gas obtained from the HTL treatment (290–360 °C for 0–30 min) varied from 40.7 to 48.3% daf, 4.7–10.4% daf, 35.6–42.1% daf, and 6.9–11.3% daf, respectively (Table 1). The most suitable models for the yields (%, daf) were selected based on the goodness of fit and significance of model terms, as expressed in Eqs. (S1–S4) in the Supplementary Material. The actual equations can be used to make predictions about the yield of products at a given reaction temperature and residence time. The coded equations were given in Eqs. (10–13) to identify the relative effects of factors by comparing the factor coefficients. Overall, reaction temperature showed a higher linear impact than residence time on the yield of all HTL products.

$$Y_{biocrude} = 48.0 + 1.2A + 0.6B - 1.4AB - 2.0A^2 - 1.7B^2 \quad (10)$$

$$Y_{hydrochar} = 6.8 - 1.2A - 0.6B + 0.5AB + 0.2B^2 - 0.9AB^2 \quad (11)$$

Table 4
ANOVA and fit statistics for the models of HTL product yield (Y).

p-value	$Y_{biocrude}$	$Y_{hydrochar}$	$Y_{aqueous}$	Y_{gas}
Model	<0.0001	<0.0001	<0.0001	<0.0001
A-Reaction temperature	<0.0001	<0.0001	0.0031	<0.0001
B-Residence time	0.0012	0.0014	0.0398	<0.0001
AB	<0.0001	0.0326	0.0010	0.3220
A^2	<0.0001	–	<0.0001	0.1081
B^2	<0.0001	0.3302	<0.0001	–
AB^2	–	0.0083	–	–
A^2B	–	–	0.1266	0.0395
Lack of Fit	0.5413	0.4287	0.4439	0.0799
Fit statistics				
R^2	0.9435	0.9302	0.9023	0.9627
Adjusted R^2	0.9217	0.9034	0.8535	0.9483
Predicted R^2	0.8801	0.8378	0.7717	0.9228
Adequate precision	20.2355	16.9013	14.1913	24.4963

– Insignificant terms ($p > 0.05$) excluded to improve models.

$$Y_{aqueous} = 36.1 - 0.6A - 0.6B + 1.0AB + 1.6A^2 + 1.5B^2 - 0.6A^2B \quad (12)$$

$$Y_{gas} = 9.3 + 1.0A + 0.6B - 0.1AB + 0.2A^2 + 0.3A^2B \quad (13)$$

where A and B were the coded factors with the high levels coded as + 1 and the low levels coded as −1.

As shown in Table 4, all the models for the yield of HTL products were found statistically significant ($p < 0.05$). The lack of fit values were not significant ($p > 0.05$) relative to the pure error, indicating that models well fit the experimental data. The goodness of fit for all models was also proven by the high values of coefficient of determination ($R^2 > 0.9$), adjusted R^2 (>0.8), and predicted R^2 (>0.7). The predicted R^2 was in reasonable agreement with the adjusted R^2 for each model, with a difference of < 0.1, suggesting sufficient terms in the model [26]. The signal-to-noise ratio (adequate precision) was also desirable (>4) for all models, which can be used to navigate the design space.

The response surface graphs in Fig. 1 showed the main and interaction effects of HTL reaction temperature and residence time on the product yield. Both experimental factors were found to have significant effects on the yield of all HTL products. Significant interaction (AB) and/or multiple interactions (AB^2 or A^2B) were also found for all yield models. As shown in Fig. 1a, at low levels of reaction temperature (e.g., 300 °C) or residence time (e.g., 4.4 min), increasing residence time or reaction temperature alone could substantially increase biocrude yield. It suggested that sufficient reaction severity (higher temperature or longer residence time) was necessary for the decomposition of sludge components (e.g., lignin and protein) and the formation of biocrude intermediates [13,14]. However, at high levels of reaction temperature (e.g., 350 °C) or residence time (e.g., 25.6 min), a limited increase of biocrude yield was shown, followed by a slight decline, when increased residence time or reaction temperature alone. This decrease was possibly due to the polymerization of biocrude intermediates into high molecular weight coke that contributed to hydrochar [27]. Another mechanism could be active secondary decomposition and enhanced gasification under higher severity [28], which led to the decrease of biocrude yield and increased the yield of aqueous and gas, as observed in

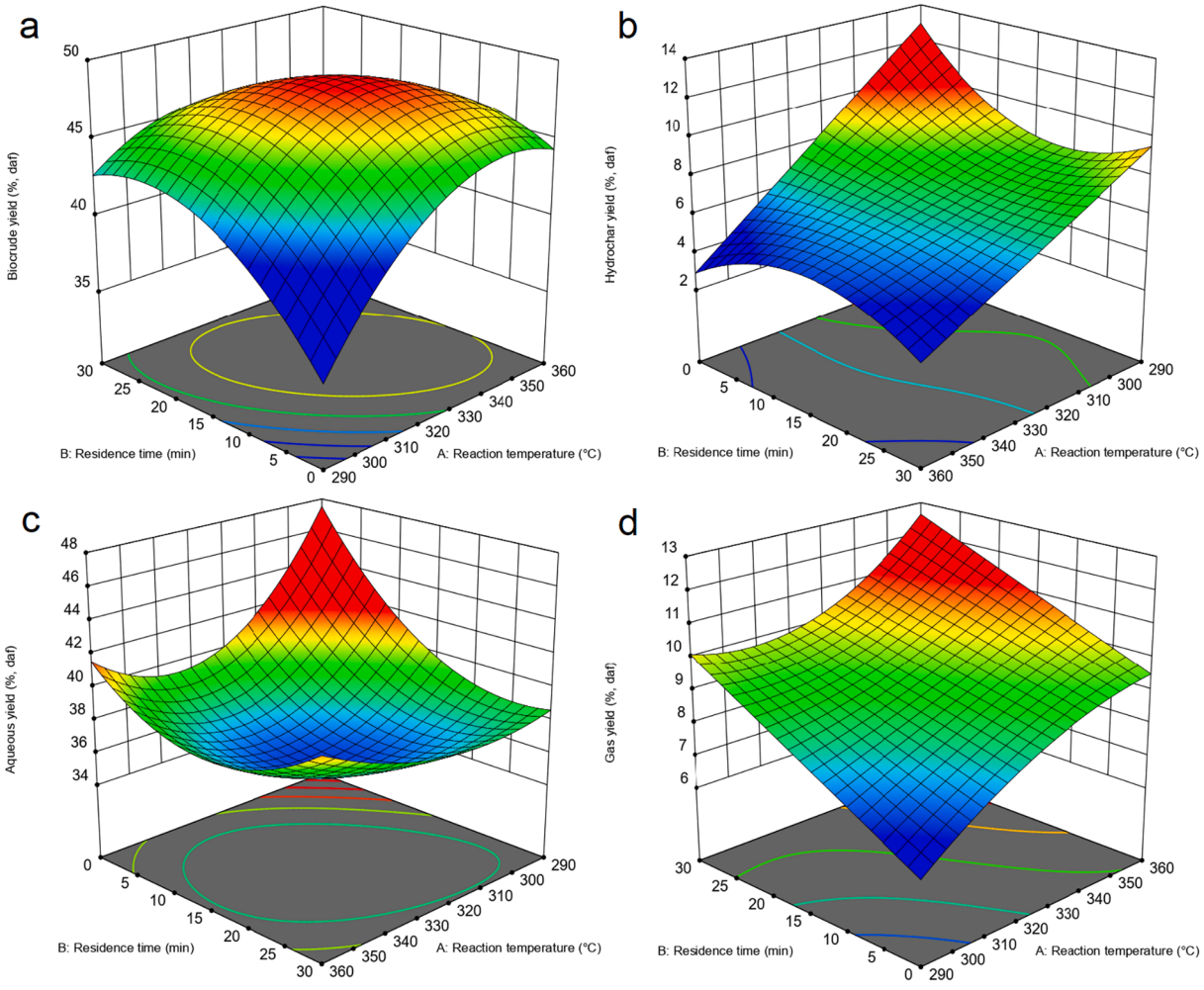

Fig. 1. Response surface plots for the yield of HTL (a) biocrude, (b) hydrochar, (c) aqueous, and (d) gas.

Fig. 1c and d. Model Eq. (10) also indicated that both temperature and residence time had positive linear effects on biocrude yield, while the negative interaction effects and secondary effects can cause the reduction of biocrude yield. Couto et al. observed that biocrude yield from digested sludge decreased at above 325 °C for 15 min [29]. Both too high and too low reaction temperature or residence time showed adverse effects on biocrude yield, with the optimal temperature range of 320–340 °C and residence time range of 10–20 min. Through modeling, the optimum conditions for maximum biocrude production were at 332 °C for 16 min, with a predicted yield of 48.2%, daf. As shown in Table 5, the predicted optimum HTL conditions were within the reported range (300–350 °C and 4–30 min) from the literature and the predicted biocrude yield was at the upper level of reported data from both batch and continuous HTL.

As a solid product, the yield of hydrochar declined constantly with increasing reaction temperature due to the conversion of organics (Fig. 1b). At low reaction temperatures (e.g., 300 °C), hydrochar yield also reduced with raising residence time and remained around 8%, daf after 15 min. At high reaction temperatures (e.g., 350 °C), hydrochar yield generally remained around 5%, daf although it slightly increased and then decreased by increasing residence time. Such a peak could be attributed to the char-forming reactions, such as condensation, cyclization, and polymerization of the aqueous product that showed the opposite trend in yield (Fig. 1c). In general, the factors showed dominant negative effects on hydrochar yield based on Eq. (11). The plot of aqueous yield (Fig. 1c) was literally inverse to biocrude yield as also revealed by the model equations, indicating the competitive distribution between aqueous compounds and biocrude components. The sum of aqueous and biocrude yield remained between 82 and 86%, daf under all conditions, suggesting that sludge was initially and primarily converted into aqueous and biocrude [34]. Linear correlation analysis indicated that the aqueous yield was negatively correlated to biocrude yield (adjusted $R^2 = 0.85$). The aqueous yield sharply decreased with increasing reaction temperature and residence time, which reached a predicted minimum of 36%, daf at 329 °C and 16.4 min close to the conditions for maximum biocrude production. Such finding is critical as it indicates that controlling HTL operating conditions could affect the partitioning of organics between biocrude and aqueous, thus maximizing biocrude production could simultaneously minimize the aqueous product and associated treatment cost in the WWTP. A similar down-and-up tendency of aqueous yield due to increasing temperature and residence time was also observed by HTL of biomass (mainly microalgae) [29]. The mechanism could be that higher reaction temperature and longer time provided sufficient energy and time to rearrange water-soluble intermediates into biocrude molecules through condensation and repolymerization [29]. However, Xu et al. found that HTL aqueous yield from secondary sludge decreased when reaction temperature raised from 260 °C to 350 °C [5], and Qian et al. reported an up-and-down pattern with increasing reaction severity [34]. The controversial results could be caused by the use of solvent (DCM) extraction of aqueous in those studies, which obtained more water-soluble organics as biocrude. Therefore, the results of this study could represent a continuous-flow HTL system where physical separation is more applicable [11]. The HTL gas yield (Fig. 1d) nearly linearly increased with reaction temperature and residence time mainly due to the decarboxylation reaction (around 98% CO_2). This positive impact was also supported by all significant terms in Eq. (13).

3.2. Elemental contents and energy recovery of biocrude

3.2.1. Elemental analysis

Elemental compositions and ash content of biocrude generated at different reaction temperatures and residence time were presented in Table 6. The HHV, ER, and EROI were also estimated. Similar to other studies [14], HTL biocrude mainly consisted of C (72.1–76.9%), H (9.1–9.7%), O (7.8–13.1%), N (4.4–4.9%), S (0.5–0.9%), and minor ash (0.1–0.4%), with an HHV of 34.8–37.2 MJ/kg. Noticeably, a linear increase of C content and a linear decrease of O content in biocrude were observed with increasing reaction temperature and residence time (Fig. 2). The linear models were significant and well fitted (Table 7). Compared to bio-oil from pyrolysis (at 450 °C for 1 h) of municipal sludge [36], which had 58.85% of C and 30.71 MJ/kg of HHV, HTL biocrude exhibited a superior quality. Considering the capacity of processing wet biomass and lower operational temperature, HTL could represent a more sustainable waste-to-energy technology than conventional pyrolysis. Due to higher contents of heteroatoms (e.g., O and N), HTL biocrude showed lower C, H, and HHV than those of petroleum with a range of 83–87%, 10–14%, and 41–48 MJ/kg, respectively [37,38]. As shown by the van Krevelen diagrams in Fig. 3, the H/C, O/C, and N/C atomic ratios in biocrude sharply decreased compared to the feedstock as a result of decarboxylation, dehydration, and denitrogenation (e.g., deamination) reactions. Also, higher reaction temperature and residence time could further reduce O/C contents in biocrude (Fig. 2). However, biocrude still contained a much higher content of O/C and N/C than petroleum mainly due to the production of oxygen functional groups from the decomposition of protein and carbohydrates and the formation of N/O-heterocyclic through Maillard reactions [39]. Therefore, upgrading biocrude using deoxygenation and denitrogenation processes, such as hydrodeoxygenation or hydrotreating, could be necessary to improve the fuel quality. Primary sludge-derived biocrude after hydrotreating could be upgraded to a quality comparable to petroleum [2].

3.2.2. Carbon and energy recovery

Fig. 4 illustrated the response surfaces for HHV, CR, ER, and EROI of biocrude, with statistical analyses shown in Table 7. The best-fitted

Table 5
Comparison of the optimum biocrude yield in this study with the literature.

Reactor type	HTL feedstock	Feedstock TS (wt%)	HTL conditions	Maximum biocrude yield (%, db)	Reference
Batch	Mixed sludge	20	332 °C, 16 min	43.3 (48.2 daf)[a]	This study
	Undigested sludge	20	300 °C, 30 min	16	[28]
	Digested sludge	9.1	325 °C, 15 min	26	[29]
	Digested sludge	25	350 °C, 20 min	21.3	[30]
	Municipal sludge	15.5	300 °C, 60 min	30.1	[31]
	Digested sludge	10	320 °C, 30 min	22.5	[32]
	Primary sludge	10	350 °C, 30 min	22	[33]
	Waste activated sludge + sawdust	10	310 °C, 10 min	33.7	[20]
	Primary sludge	2.2	350 °C, 4 min	30.9	[34]
	Secondary sludge	10	340 °C, 20 min	23	[5]
	Undigested sludge	10	350 °C, 30 min	32.3	[35]
	Primary sludge	9	330 °C, 10 min	43.4	[19]
Plug-flow continuous	Primary sludge	16	325 °C, 9 min	40.8	[11]

[a] predicted values.

Table 6
Quality of biocrude from municipal mixed sludge under various HTL conditions.[a]

Run	Reaction temperature (°C)	Residence time (min)	Ultimate analysis (%)					Ash (%)	HHV (MJ/kg)	ER (%)	EROI
			C	H	N	S	O				
1	325	15	74.2	9.3	4.8	0.8	10.6	0.3	35.4	69.1	2.42
2	350	25.6	75.8	9.6	4.8	0.5	8.9	0.4	37.0	68.5	2.22
3	300	25.6	74.7	9.6	4.4	0.8	10.4	0.1	36.0	65.2	2.49
4	300	25.6	73.6	9.4	4.8	0.7	11.1	0.4	35.8	66.7	2.54
5	350	4.4	74.0	9.2	4.7	0.7	11.1	0.3	36.1	67.6	2.19
6	300	4.4	72.8	9.3	4.6	0.8	12.3	0.2	34.9	57.5	2.19
7	325	15	74.6	9.3	4.8	0.8	10.2	0.3	35.4	69.4	2.43
8	350	25.6	76.9	9.5	4.9	0.6	7.8	0.3	36.9	67.0	2.17
9	300	4.4	73.1	9.1	4.8	0.6	12.2	0.2	34.8	57.9	2.21
10	350	4.4	73.9	9.4	4.8	0.8	10.8	0.3	35.8	67.8	2.19
11	360	15	76.6	9.6	4.6	0.7	8.3	0.2	37.2	68.2	2.14
12	290	15	72.1	9.3	4.5	0.8	13.1	0.2	35.3	62.0	2.46
13	325	0	74.3	9.6	4.8	0.9	10.2	0.2	35.8	62.7	2.20
14	325	15	75.4	9.1	4.8	0.6	9.9	0.2	35.3	68.2	2.39
15	360	15	75.6	9.7	4.8	0.9	8.8	0.2	36.8	68.7	2.16
16	290	15	73.9	9.3	4.7	0.8	11.0	0.3	35.9	60.7	2.41
17	325	0	73.7	9.5	4.6	0.9	11.2	0.1	35.4	63.8	2.24
18	325	30	75.1	9.5	4.6	0.7	9.9	0.2	36.5	66.4	2.33
19	325	30	75.4	9.5	4.6	0.6	9.6	0.3	36.9	68.0	2.38

[a] HHV = higher heating value; ER = energy recovery; EROI = energy return on investment.

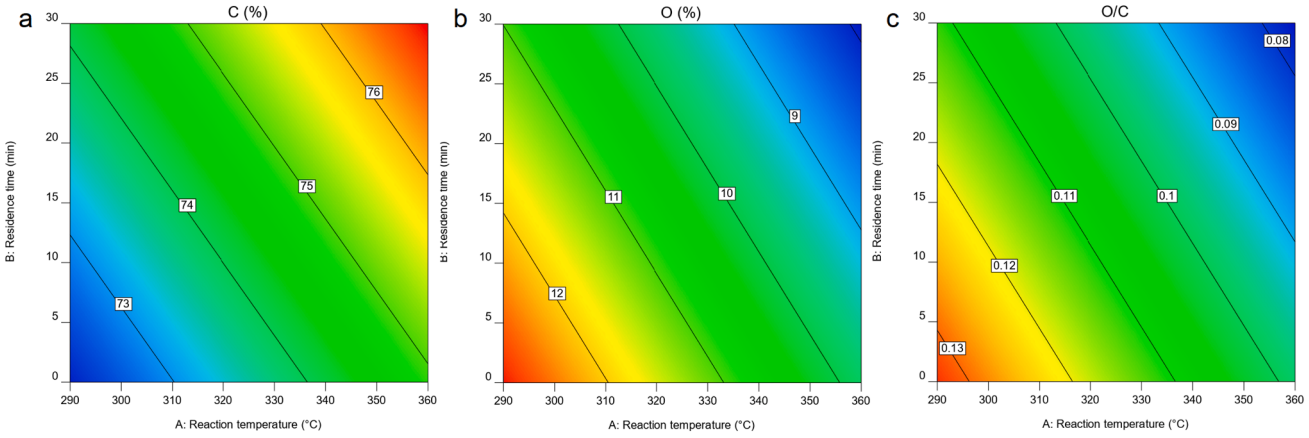

Fig. 2. Contour plots for (a) C content, (b) O content, and (c) O/C atomic ratio of biocrude.

Table 7
ANOVA and fit statistics for the models of biocrude quality.

p-value	C	O	O/C	HHV	CR	ER	EROI
Model	<0.0001	<0.0001	<0.0001	<0.0001	<0.0001	<0.0001	<0.0001
A-Reaction temperature	<0.0001	<0.0001	<0.0001	<0.0001	<0.0001	<0.0001	<0.0001
B-Residence time	0.0007	0.0009	0.0011	<0.0001	<0.0001	<0.0001	<0.0001
AB	–	–	–	–	<0.0001	<0.0001	<0.0001
A^2	–	–	–	0.0010	<0.0001	<0.0001	<0.0001
B^2	–	–	–	0.0062	<0.0001	<0.0001	<0.0001
A^2B	–	–	–	–	0.0045	–	–
Lack of Fit	0.5367	0.3008	0.3384	0.1102	0.8715	0.2491	0.1478
Fit statistics							
R^2	0.7638	0.7884	0.7802	0.9061	0.9876	0.9634	0.9570
Adjusted R^2	0.7342	0.7620	0.7527	0.8793	0.9814	0.9494	0.9404
Predicted R^2	0.6623	0.6900	0.6791	0.8211	0.9656	0.9222	0.9085
Adequate precision	12.6158	13.3736	13.0630	14.8372	38.1381	22.2585	20.1838

– Insignificant terms ($p > 0.05$) excluded to improve models.

models (Eqs. S5–S8) were listed in the Supplementary Material. The coded equations were presented below:

$$Biocrude\ HHV = 35.38 + 0.53A + 0.46B + 0.39A^2 + 0.30B^2 \quad (14)$$

$$Biocrude\ CR = 67.67 + 2.50A + 1.01B - 1.68AB - 2.85A^2 - 2.51B^2 + 0.861A^2B \quad (15)$$

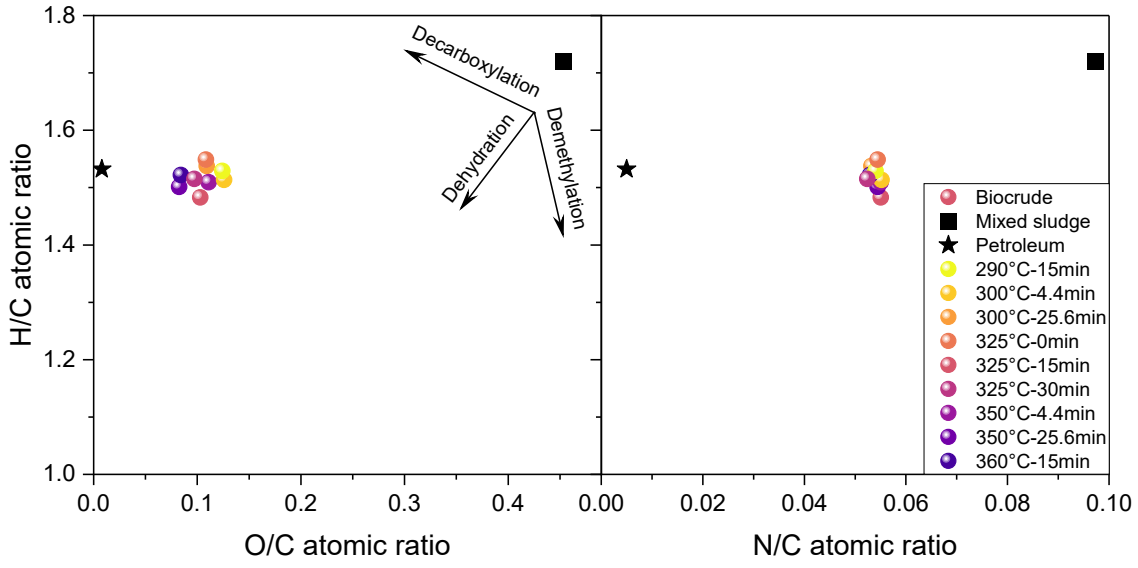

Fig. 3. van Krevelen diagram of biocrude from various HTL conditions, compared to feedstock (mixed sludge) and petroleum crude oil [39].

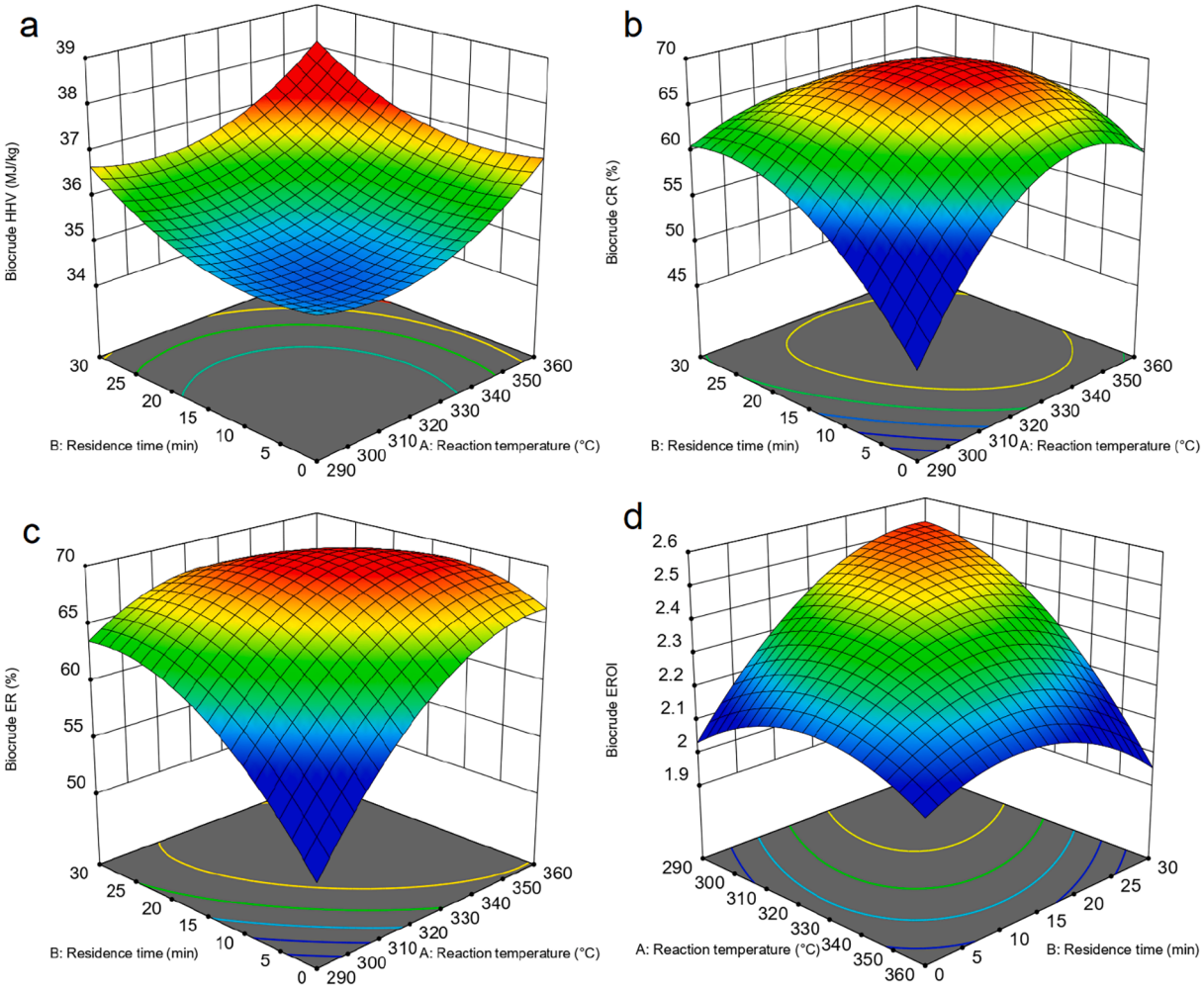

Fig. 4. Response surface plots for (a) HHV, (b) CR, (c) ER, and (d) EROI of biocrude from HTL of mixed sludge.

$$Biocrude\ ER = 78.78 + 2.80A + 1.78B - 2.09AB - 2.14A^2 - 1.96B^2 \quad (16)$$

$$Biocrude\ EROI = 2.41 - 0.092A + 0.064B - 0.078AB - 0.065A^2 - 0.067B^2 \quad (17)$$

where, A and B were the coded factors.

As shown in Fig. 4a, biocrude HHV increased notably when the reaction temperature and/or residence time increased, with the maximum HHV (37.2 MJ/kg) obtained at 360 °C for 15 min. However, the model predicted that higher HHV could be achieved at higher reaction severities. The findings were in agreement with the literature. Silva Thomsen et al. conducted HTL of primary sludge with a plug-flow continuous system and found that biocrude HHV increased from 30.2 to 34.6 MJ/kg within the temperature range of 300–350 °C [11]. Increasing residence time from 0 to 30 min was found to enhance biocrude HHV produced at both subcritical (325 °C) and supercritical (375 °C) conditions [40]. The increase of biocrude HHV could be benefited from the removal of O by enhanced decarboxylation, dehydration, and recombination reactions [14]. The coded Eq. (14) also suggested that reaction temperature and residence time showed comparable impacts on improving biocrude HHV, while no significant interaction effects were found.

The biocrude CR (Fig. 4b) and ER (Fig. 4c) showed response surfaces fairly similar to biocrude yield (Fig. 1b) regarding the effects of reaction temperature and residence time. Both biocrude CR and ER increased first and then decreased when increasing reaction temperature or residence time alone, which varied at 56.6–68% and 59.1–71.3%, respectively. Such trends were mainly related to the change of biocrude yield. Fig. 5 demonstrated that biocrude ER had a linear correlation to biocrude yield and CR, with an adjusted R^2 of 0.87 and 0.95, respectively. This indicated that, to some extent, biocrude yield or CR could be used to predict biocrude ER which is a more representative measurement for both quantity and quality of biocrude. Sudibyo et al. also stated that all investigated factors showed identical impacts on biocrude CR and ER to those for biocrude yield from HTL of acid whey at a temperature range of 280–360 °C [41]. Although biocrude HHV improved with increasing reaction severity, biocrude yield dropped after 332 °C for 16 min. As a result, the model predicted that maximum biocrude CR (68.2%) and ER (70.8%) could be reached at a moderate condition (332 °C for 16.9 min) close to those for maximum biocrude yield. Compared to the previous study by PNNL using sludge from the same WWTP, although having similar elemental contents and energy densities, the biocrude ER from mixed sludge (up to 70.8%) was notably higher than that from primary (63.5%), secondary (34.9%), and digested sludge (41.3%) [2]. This highlighted the importance of process optimization. Meanwhile, the balance of carbohydrates and proteins in the mixed sludge also promoted the Maillard reaction and thus contributed to the higher biocrude yield and ER. It was reported that Annacis Island WWTP primary sludge contained 50.55% of carbohydrates and 21.74% of protein while secondary sludge had 15.72% of carbohydrates and 50.97% of protein on a dry basis [42]. As a result, their mixture (mixed sludge) could have a carbohydrate to protein mass or molar ratio close to 1:1 where the greatest synergetic effect from the Maillard reaction could occur [18].

The EROI was estimated by considering the energy output from biocrude over the main energy input only for heating the reactor during HTL. As shown in Fig. 4d, the EROI went up and down at low reaction temperatures (e.g., 300 °C) or short residence time (e.g., 4.4 min) when residence time or reaction temperature was increased alone, whereas it decreased sharply with increasing reaction temperature or decreasing residence time at long residence time (e.g., 25.6 min) or high reaction temperatures (e.g., 350 °C), respectively. This suggested that a low reaction temperature for a long residence time would be beneficial for enhancing EROI. In fact, the EROI was improved in two ways: 1) Maximizing the energy output (i.e., biocrude ER) by adjusting HTL conditions; and 2) minimizing the energy input that was directly linked to reaction temperature. The EROI was found to vary between 2.14 and 2.54 at all experimental conditions, suggesting that HTL of municipal sludge could be net energy positive (EROI > 1). The values were in the range of 1.6–3.4 from a continuous HTL processing primary sludge (16 wt% solids) [11]. An earlier study used the same feedstock but only achieved 0.5 of EROI, which was caused by the low solids content (4 wt %) of the feedstock, while heat exchangers could be employed to HTL systems to significantly improve the EROI [43].

3.2.3. *Multicriteria optimization and model validation*

Using the above-mentioned models, optimization of sludge-to-biocrude conversion was performed on three different objectives: 1) Maximum CR and ER regardless of the energy consumption, 2) maximum EROI disregarding others, and 3) balancing ER and EROI. As shown in Table 8, by entering constraints of “maximize” and “in range” (with their importance level from 1 to 5) for dependent variables in Design Expert, the optimum HTL operating conditions were determined and the target values were predicted by the desirability approach. Desirability close to 1 suggests an acceptable prediction, while desirability close to 0 indicates an unacceptable prediction. It demonstrated that all three objectives could be achieved with desirable results (desirability > 0.8), while Objective 1 can be reached with the highest desirability (=1). Among the three objectives, max CR (68.2%) and ER (70.8%) were obtained at a higher reaction temperature (332 °C for 16.9 min), whereas max EROI (2.52) was observed at a lower temperature (300 °C for 25.6 min). As expected, an ER-EROI balance was reached at an intermediate temperature (320 °C for 21.1 min).

Additional experiments employing the optimum conditions for max

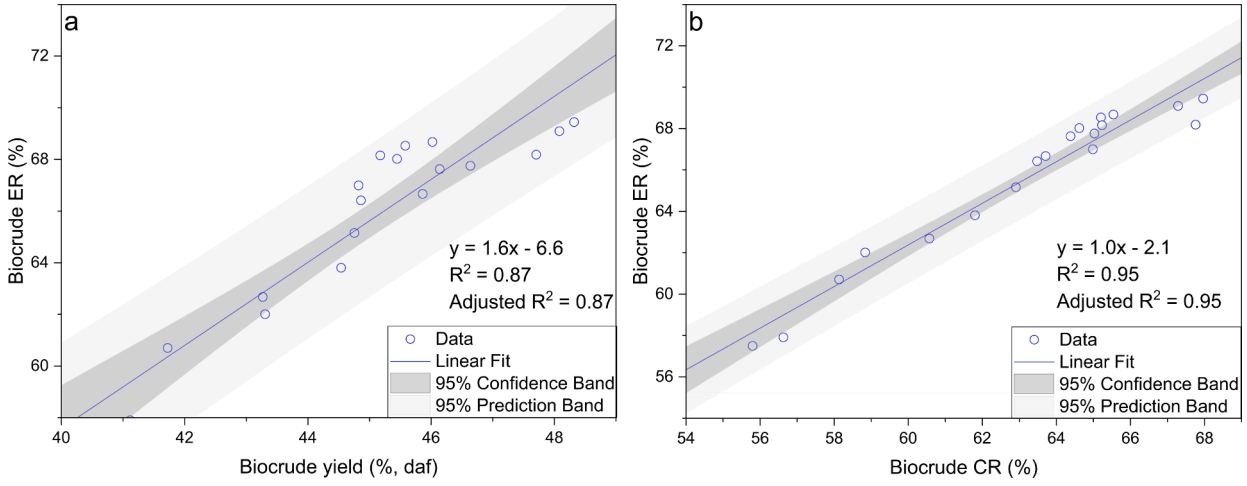

Fig. 5. Correlation analysis of (a) biocrude ER vs yield and (b) biocrude ER vs CR.

Table 8
Multicriteria optimization for different objectives.

Objective	Dependent Variables			Optimum conditions			Target values		
	Biocrude CR	Biocrude ER	Biocrude EROI	Reaction temperature (°C)	Residence time (min)	Desirability	Biocrude CR (%)	Biocrude ER (%)	Biocrude EROI
1. Max CR & ER	Maximize (+++++)	Maximize (+++++)	In range	332	16.9	1.00	68.2	69.7	2.39
2. Max EROI	In range	In range	Maximize (+++++)	300	25.6	0.93	63.3	66.0	2.52
3. Max ER & EROI	In range	Maximize (+++++)	Maximize (+++)	320	21.1	0.88	67.0	68.9	2.45

Table 9
Comparison of predicted and experimental values (mean ± standard deviation) at the optimum conditions (332 °C and 16.9 min) for maximum biocrude CR and ER.

Response	Predicted values	95% prediction interval	Experimental results
Biocrude yield (%, daf)	48.2 ± 0.6	47.0–49.4	48.9 ± 0.7
Hydrochar yield (%, daf)	6.4 ± 0.5	5.5–7.3	6.5 ± 0.2
Aqueous yield (%, daf)	36.0 ± 0.7	34.7–37.3	34.7 ± 0.3
Gas yield (%, daf)	9.7 ± 0.3	9.2–10.2	10 ± 1
Biocrude HHV (MJ/kg)	35.7 ± 0.3	35.2–36.2	35.7 ± 0.1
Biocrude CR (%)	68.2 ± 0.5	67.2–69.1	69 ± 2
Biocrude ER (%)	69.7 ± 0.8	68.0–71.3	70.8 ± 0.8
Biocrude EROI	2.39 ± 0.03	2.33–2.45	2.42 ± 0.03

CR and ER were performed in duplicate to validate the accuracy, reliability, and practicability of the regression models. Compared to the model predicted values in Table 9, the experimental results of biocrude yield, hydrochar yield, gas yield, and biocrude HHV/CR/ER/EROI were slightly higher, while aqueous yield was lower. However, all experimental results were well within 95% prediction interval of the predicated mean, indicating accurate predictabilities of the developed models.

3.3. Characterization of biocrude

3.3.1. Total acid number (TAN)

TAN measures the number of acidic substances in biocrude, which is typically used as quality control of petroleum products. The acidic constituents in oil could be organic (e.g., esters, phenolic compounds, lactones, and resins) and inorganic acids (e.g., salts of heavy metals). Those acids in biocrude could cause potential corrosion issues in storage and refinery and thus it is essential to reduce the TAN [44]. TAN in biocrude from HTL of mixed sludge varied between 48.6 and 63.6 mg KOH/g biocrude. The values were consistent with a previous study by PNNL, which performed a plug-flow continuous HTL (276–358 °C for 18–30 min) using sludge from the same WWTP. The TAN in biocrude from primary, secondary, and digested sludge was found to be 65, 44.8, and 36 mg KOH/g, respectively [2]. The variations might be caused by the different biochemical compositions in the feedstock. Biocrude obtained from lipid-rich (>30 wt%) algae showed a high TAN (101–118 mg KOH/g), while protein-rich (>45 wt%) algae-derived biocrude resulted in a low TAN (25–48 mg KOH/g) [45].

Table 10
ANOVA and fit statistics for the model of biocrude TAN.

Source	p-value	Fit statistics	Value
Model	<0.0001	R^2	0.9787
A-Reaction temperature	<0.0001	Adjusted R^2	0.9652
B-Residence time	<0.0001	Predicted R^2	0.9329
AB	0.0013	Adequate precision	22.1024
A^2	<0.0001		
B^2	<0.0001		
A^2B	0.0391		
AB^2	0.0003		
Lack of Fit	0.5877		

According to Table 10, reaction temperature, residence time, and their interactions showed significant effects on TAN levels of biocrude. The reduced cubic model expressed by Eq. (S9) was found with excellent goodness of fit and predictability. The coded equation Eq. (18) suggested the effects of experimental terms. Both HTL reaction temperature and residence time showed negative linear and interactive impacts but positive quadratic effects on TAN.

$$TAN = 51.15 - 2.00A - 3.39B - 1.42AB + 3.34A^2 + 3.20B^2 + 1.10A^2B - 2.47AB^2 \quad (18)$$

where A and B were the coded factors.

The response surface plot (Fig. 6) revealed that the raising reaction temperature within the range of 290–330 °C could significantly reduce biocrude TAN and reached equilibrium at 330–360 °C regardless of residence time. Many other studies also supported that increasing reaction temperature between 250 and 320 °C had negative impacts on biocrude TAN [45–47]. The decrease of TAN could be attributed to further decarboxylation of organic acids (e.g., fatty acids and carboxylic acids) under a more severe environment. However, HTL of coconut shell at 270–330 °C obtained biocrude with a TAN (180–190 mg KOH/g) nearly doubled that from 240 °C (98 mg KOH/g) [46]. It was suggested that more acetic acid and phenolics were formed at higher temperatures by hydrolysis and rehydration and contributed to higher TAN. Carbohydrate-rich biomass tends to form more acids during HTL, while mixed sludge has a more balanced composition of protein and

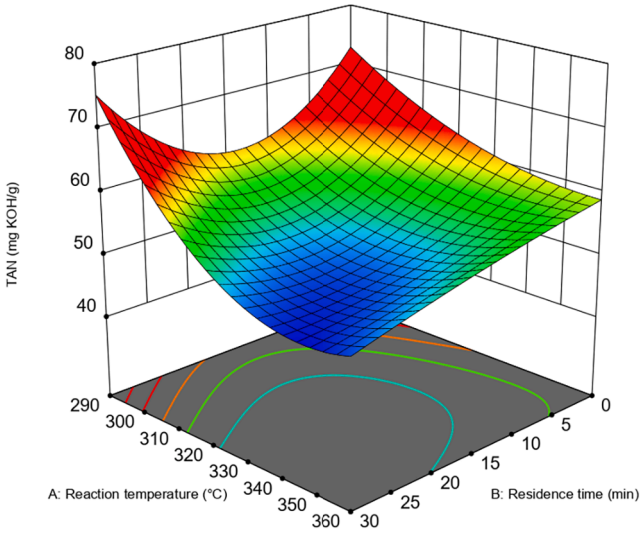

Fig. 6. Response surface plot for total acid number (TAN) of biocrude from HTL of mixed sludge.

carbohydrate to generate less acids. The residence time had different effects on biocrude TAN at a low or high reaction temperature. Increasing residence time, biocrude TAN showed a down and up trend at a low temperature (e.g., 300 °C), while it decreased constantly at a high temperature (e.g., 350 °C). Similar tendencies were also observed for the HTL of municipal sludge at 325 and 400 °C [48]. Although biocrude TAN could be reduced by controlling reaction conditions and adding catalysts, such as transition metal chlorides [46] and bases (e.g., NaOH and Na_2CO_3) [47,49], it is generally much higher than the standard specifications for commercial fuels, such as ≤ 0.1, ≤0.3, and ≤ 0.5 mg KOH/g for aviation turbine fuels (ASTM D7566–20c), fuel oils grade B6–B20 (ASTM D396–21), and distillate marine fuels (ISO 8217:2017), respectively. Therefore, upgrading biocrude for TAN reduction is necessary prior to its application or refining. Esterification was found to effectively decrease biocrude TAN from 40 to < 1 mg KOH/g [50], and hydrotreating could reduce it to < 0.01 mg KOH/g [2].

3.3.2. *Chemical compositions by GC–MS*

Biocrude samples obtained from different hydrothermal conditions were analyzed by GC–MS to discover the compositional changes and potential reaction pathways regarding HTL reaction temperature and residence time. Based on the TIC graph (Fig. S2), more than fifty organic compounds were identified in biocrude. For biocrude generated from different reaction temperatures (290–360 °C) and residence time (0–30 min), their compositions (identified peaks) were comparatively similar while their relative contents varied. It should be noted that the GC–MS results only provided information about isopropanol-soluble molecules that were light enough to vaporize and pass through the GC column.

Based on the presence of heteroatoms, the identified compounds can be categorized into nitrogenous (containing N), oxygenated (containing O but no N), and hydrocarbons groups (containing only C and H). Their relative percentages in biocrude samples from various HTL conditions were summarized in Fig. 7a–b. The biocrude primarily consisted of N-containing compounds (>46%), followed by oxygenated groups (26–30%) and hydrocarbons (16–27%). Increasing reaction temperature could greatly reduce nitrogenous compounds and generate more hydrocarbons, while residence time did not seem to have a significant impact on the composition. The C–N bonds at higher temperatures are much more reactive, which probably caused the partitioning of N to aqueous phase and benefited the generation of more hydrocarbons in biocrude [51]. The N/O-containing compounds included amides and N-heterocycles (e.g., indoles and pyrrolidines), which could be generated from the deamination, cyclization, and condensation of amino acids (hydrolyzed from proteins) [18,52,53]. Pyrazines and their derivates have not been identified from HTL of pure protein [16,18]. Their detection in sludge-derived biocrude suggested the occurrence of Maillard reactions between amino acids and reducing sugars (e.g., monosaccharides hydrolyzed from larger carbohydrates). The oxygenated compounds mainly consisted of amides, alcohols, esters, ketones, phenols, acids, and some N-heterocycles, while hydrocarbons were mostly alkenes (>11%) with little alkanes (<2%).

The major chemical groups can be further divided as shown in Fig. 7c–d. Among the classified groups, carboxylic acids derived from the hydrolysis of lipids, the deamination of amino acids, and the decomposition of monosaccharides, played important roles as the reaction intermediates. They could transform into alcohols, ketones, and hydrocarbons through decarboxylation, form esters by esterification with alcohols, or produce amides through acylation with ammonia or amines (from the deamination of amino acids) [54]. Amides (>31%) were found the most abundant in biocrude, as agreed with a previous study about mixed sludge-derived biocrude [55]. The amides were mainly straight aliphatic (e.g., hexadecanamide, octadecanamide, and 9-octadecenamide, (Z)-), which could be formed from the acylation of carboxylic acids with amines or ammonia [16,56] or the aminolysis of esters with amines or ammonia [57]. Some cyclic amides, such as octanoic acid, morpholide, could be generated from the cyclization of alcohols, ammonia, and amino acids [52]. The fatty acids hydrolyzed from lipids (predominantly from primary sludge) could undergo decarboxylation to produce long-chain alkenes (e.g., 1-tetradecene, 1-pentadecene, and 9-octadecene, (E)-) [33]. Unlike the lignin-rich feedstocks (e.g., rice straw) that tended to produce many phenolic compounds (>33%) [58], the relative content of phenols in sludge-derived biocrude was relatively low (<6.2%). Although phenolic compounds are mainly generated from the degradation of lignin, phenols could be formed through dehydration and cyclization of monosaccharides or the condensation and cyclization of amino acids [59].

Fig. 7c showed the effects of HTL reaction temperature on the major chemical groups in biocrude. As the temperature increased from 290 to 360 °C, the primary compounds including amides, N-heterocycles, and alcohols dramatically decreased, while other components (e.g., alkenes, esters, ketones, and phenols) increased. Such changes generally lead to the reduction of oxygen content in biocrude probably due to the enhanced decarboxylation reactions at higher temperatures. The decrease of amides could be caused by the competitive formation of hydrocarbons from the decarboxylation of fatty acids [16]. The esters-forming reactions (e.g., 4-Cyanobenzoic acid, hexadecyl ester) could decrease the generation of alcohols and restrain the production of amides by occupying ammonia and amino acids [54]. The reduction of N-heterocycles mainly resulted from the decrease of pyrazines (e.g., methyl-pyrazine and ethyl-pyrazine). Fan et al. observed a similar trend for the HTL (250–350 °C) of lysine and lactose mixture [60]. It was indicated that melanin polymer instead of biocrude components was

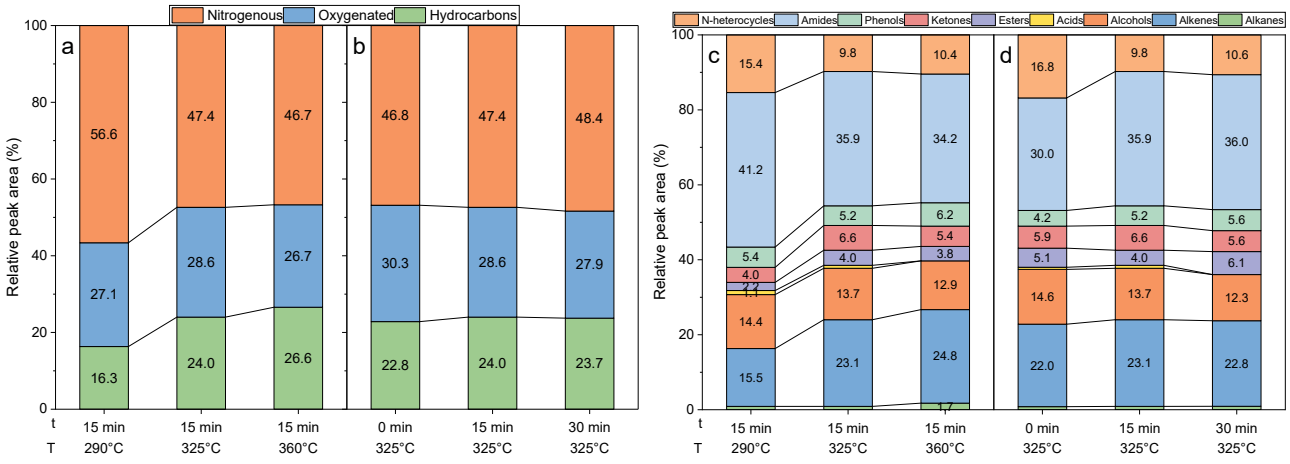

Fig. 7. Chemical composition of biocrude samples produced at various reaction temperatures (T) and residence time (t).

generated by Maillard reactions at a lower temperature (260 °C), which would decompose into monocyclic compounds (e.g., pyrazines) when the temperature increased to 280 °C; on the other hand, further increasing temperature could likely cause the decomposition of pyrazines [61]. However, to the best of our knowledge, there is no clear pathway to the decomposition of pyrazines in the literature. The decrease of alcohol was caused by the enhanced dehydration reactions at higher temperatures, which would form more alkenes. The increase of cyclic ketones (mainly 4.alpha., 5-Cyclo-A-homo-5.alpha.-cholestan-6-one) by increasing temperature could be attributed to the rearrangement reactions of furan derivatives from monosaccharides [57]. The higher temperature (360 °C) also resulted in more phenols for their high stability due to combination reactions of intermediates, such as furfurals and amino acids [16,57].

As shown in Fig. 7d, the chemical composition of biocrude was also affected by the HTL residence time. Obvious decreases of N-heterocycles and alcohols and an increase of amides were observed when increasing residence time from 0 to 30 min. Similar to the effect of temperature, the reduction of N-heterocycles was mainly caused by the loss of pyrazines, indicating its decomposition with time at a high temperature (325 °C). The presence of lipids could suppress Maillard reactions due to the competition of amide-forming reactions between fatty acids and sugar-derived carbonyl compounds [60]. This could be responsible for the enhanced contents of amides with longer residence time. The biggest change among alcohols was cholesterol which dropped from 5% at 0 min to 0.8% at 30 min, which was probably dehydrated into alkenes (e.g., cholest-4-ene) [62] and then furthered oxidized into ketones (e.g., 4.alpha.,5-Cyclo-A-homo-5.alpha.-cholestan-6-one) [51]. The other chemical groups (e.g., hydrocarbons, phenols, and ketones) increased slightly due to longer time for the reactions among intermediates.

3.3.3. *Pyrolysis and oxidation behaviors by TGA–DSC*

The pyrolysis characteristics of biocrude were analyzed by TGA–DSC under N_2 environment and presented in Fig. 8a-b. Based on the derivative thermogravimetry (DTG) and DSC curves, two distinct reaction stages could be identified: 1) distillation – evaporation and decomposition of volatile compounds in the first wide region from initial temperature to around 300 °C, where the heat flow was relatively steady; 2) cracking – once reaching certain temperature (>290 °C), remaining heavier compounds start visbreaking and thermal cracking reactions and release cracking gas, showing a large endothermic peak [63–65]. The reaction regions and mass losses, with the residue at the end of cracking during pyrolysis were summarized in Table 11. The primary weight loss (>50%) was found in the distillation region, which increased with HTL reaction temperature and/or residence time. On the contrary, the mass changes of cracking and the residue amounts decreased with HTL reaction temperature and/or residence time. Noticeably, the distillable fractions and residue of biocrude were comparable to heavy crude oils [66,67], suggesting a good substitute for fossil fuels. The weight loss below 100 °C was attributed to dehydration and evaporation of light volatiles, while the molecules of C5–C30 as identified by GC–MS (such as pyrazines, alcohols, hydrocarbons, etc.) were responsible for the mass changes between 100 and 300 °C [56,68]. It was suggested that aromatics, resin, and asphaltene could contribute to the cracking stage [64,69].

Compared to the pyrolysis, biocrude oxidation showed three stages

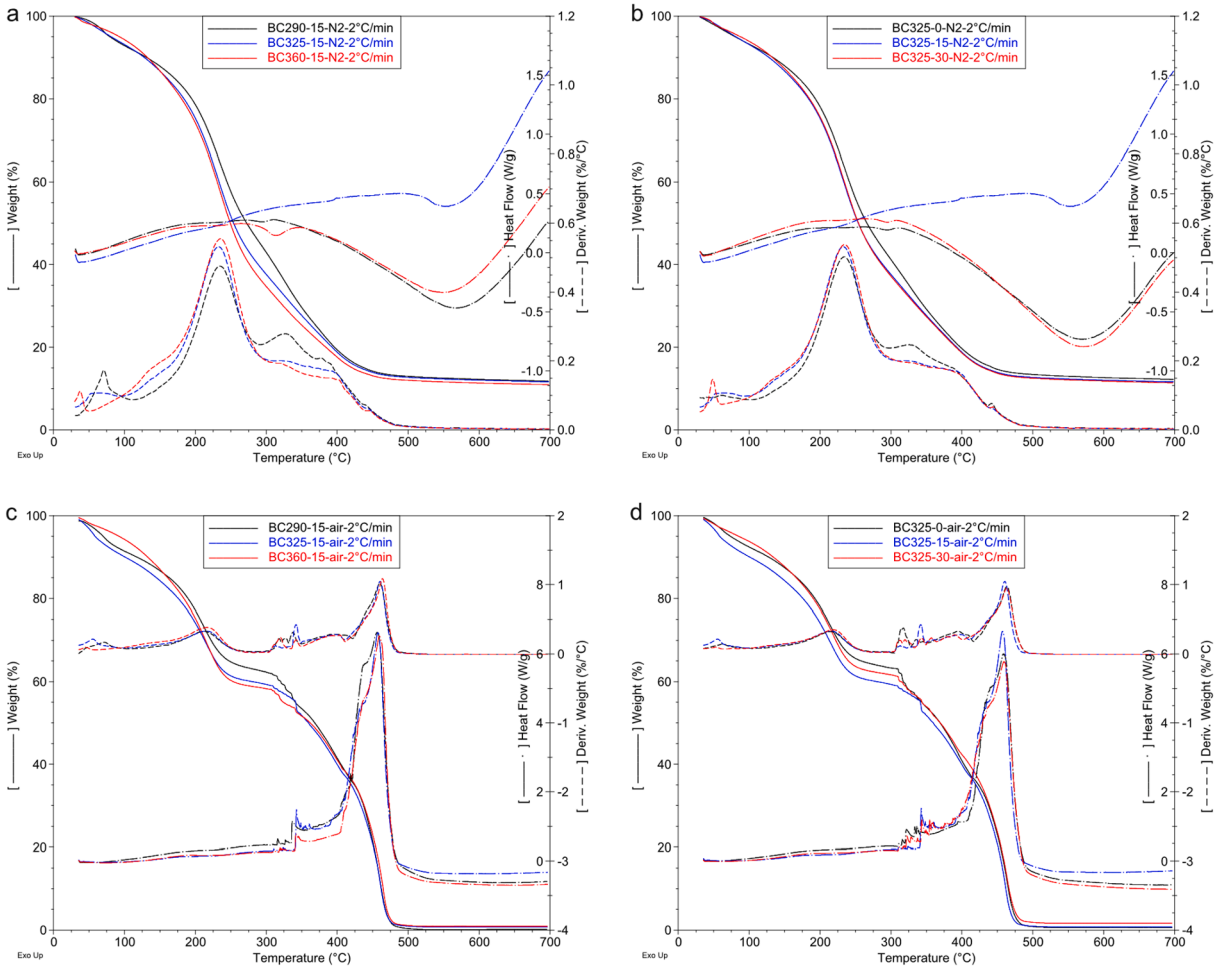

Fig. 8. TG-DTG-DSC curves of biocrude under N_2 (a-b) and air (c-d) atmosphere at a heating rate of 2 °C/min.

Table 11
Reaction regions, mass losses (Δm), and enthalpy of reactions (ΔH) during pyrolysis and oxidation of biocrude.

Biocrude sample	HTL conditions		Pyrolysis					Oxidation[a]						
			Distillation		Cracking		Residue (%)	LTO		FD			HTO		
	T (°C)	t (min)	Region (°C)	Δm (%)	Region (°C)	Δm (%)		Region (°C)	Δm (%)	Region (°C)	Δm (%)	ΔH (J/g)	Region (°C)	Δm (%)	ΔH (J/g)
BC290-15	290	15	30–290	54.7	290–567	32.9	12.5	30–299	37.6	299–419	26.7	–2233	419–522	35.5	–8672
BC325-0	325	0	30–296	57.9	296–570	29.2	12.9	30–304	36.7	304–417	26.7	–1776	417–522	35.9	–9146
BC325-15	325	15	30–306	63.6	306–551	24.0	13.4	30–304	40.8	304–410	20.0	–1913	410–521	36.3	–8707
BC325-30	325	30	30–315	65.8	315–569	22.1	12.0	30–304	38.5	304–400	19.3	–1699	400–523	40.5	–10219
BC360-15	360	15	30–314	68.0	314–549	20.3	11.7	30–302	41.7	302–410	19.7	–1057	410–518	37.5	–9135

[a] LTO – low temperature oxidation; FD – fuel deposition; HTO – high temperature oxidation.

(Fig. 8c-d): 1) low-temperature oxidation (LTO) – heterogeneous oxidation reactions between 30 and 300 °C occur between gas and liquid phases, along with evaporation of volatiles; 2) fuel deposition (FD) – a transition stage between 300 and 400 °C when thermo-oxidative cracking reactions happen and leave coke depositions as fuel; 3) high-temperature oxidation (HTO) – the primary combustion of heavier components and deposited coke from FD stage and generates a large amount of heat as shown by DSC [64,65,70]. The temperature ranges of the first two oxidation stages were similar to pyrolysis, while the pyrolysis cracking region was split into FD and HTO. LTO generally involves oxygen addition (forming hydroperoxides), and isomerization and decomposition of formed hydroperoxides [70]. The most weight loss (36–42%) was still in LTO, but it was much less than that of pyrolysis distillation (Table 11). FD reactions include breaking of C–C and C-heteroatom bonds, rupture of alkyl side chains, and dehydrogenation and ring-opening of naphthene and aromatics [71]. With increasing HTL reaction severities, the weight loss decreased during FD but increased in the HTO stage, and thus generated less heat (ΔH) at FD and more heat during HTO. More superior combustion performance of biocrude could be achieved by more severe HTL reaction conditions. It was indicated that resins and asphaltenes were the main contributors to the heat release in FD and HTO regions [71,72]. The asphaltene fraction has been identified in HTL biocrude derived from algae, food waste, wood, and primary sludge [73–75]. Asphaltenes are polycyclic and heterocyclic aromatics that can be formed through condensation and polymerization of intermediates from the Maillard reaction and aromatics degraded from lignin [75,76]. Notably, the oxidation DTG-DSC behaviors of biocrude were found to be identical to crude oils [77]. However, the heat of combustion during HTO was found to be much higher than that from crude oils [71] but between resins [78] and asphaltenes [79]. This suggested that sludge-derived biocrude may contain abundant resins and asphaltenes, which could affect the refining process, especially asphaltenes (catalyst deactivation by coking).

3.3.4. *Trace elements and contaminants*

ICP-MS analysis was conducted to identify the other elements in biocrude besides major elements (CHNSO). It was found that most other elements were at trace levels (<0.1 wt% or 1000 mg/kg) in biocrude derived from mixed sludge. Fig. 9 displayed the impacts of reaction temperature (290–360 °C) and residence time (0–30 min) on various trace elements in biocrude. Many trace elements did not exhibit significant but slight changes at different HTL conditions. Noticeably, enhancing temperature could reduce the content of Zn, K, and As but increase Cu, Ni, Cr, and V, whereas extending residence time would decrease As but increase Ca, Ni, Cr, Ba, Mn, Co, and V. The mechanisms behind these changes are not clear and require further studies. However, employing fast HTL (no ramping) on microalgae at 350 °C, Jiang and Savage observed different effects that Mg and P in biocrude dropped 13 and 38 times, respectively, by increasing residence time from 1 min to 3 min, while Fe reached the highest concentration at 10 min and then gradually decreased [80]. They also reported that after 5 min, most elements (e.g., P, Mg, Ca, K, and Cu) in biocrude did not vary much with time. The present study could not witness such significant impacts, probably due to the equilibrium during the ramping period of isothermal HTL. Another study suggested that As in algae-derived biocrude followed an exponential growth with increased reaction severity (220–360 °C for 15–25 min) [81]. The opposite observation could be because their investigation was based on arsenic acid as As(V) that would be converted into more mobile As(III) under the reduction environment (Eh ≤ –45 mV).

Among the examined elements, Fe (497–656 mg/kg) was found the most abundant, followed by Ca, P, Al, Zn, Cu, Mg, K, and Ni that were in the range of 6–231 mg/kg, while the others were at 1–6 mg/kg (e.g., Cr, Ba, Mn, Mo, As, Co, Se, and V) or < 1 mg/kg (e.g., Hg and Pb), and Cd

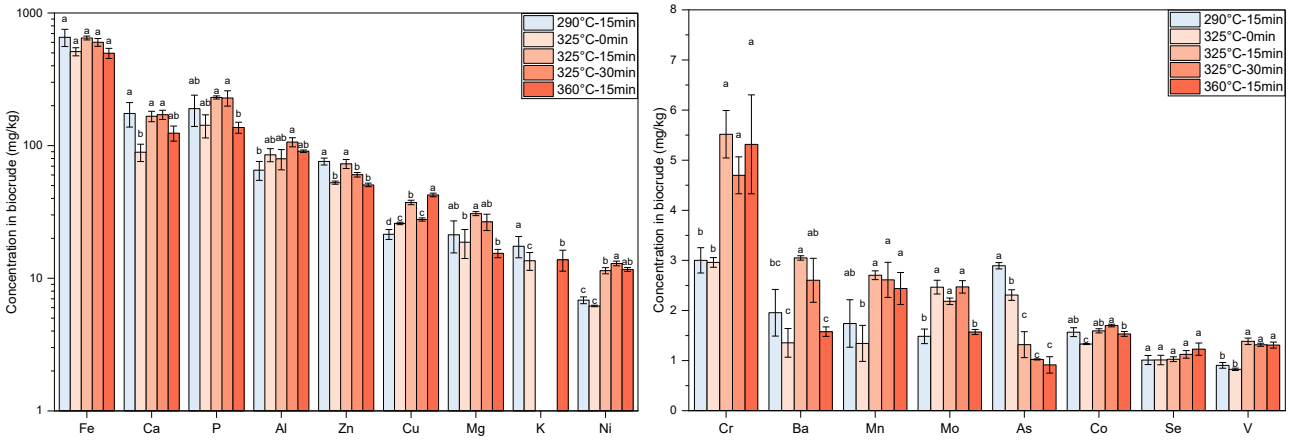

Fig. 9. Effects of HTL conditions on concentrations of trace elements in biocrude from mixed sludge (detection limit: K < 12 mg/kg). For each element, different letters above columns indicate a significant difference at $p < 0.05$ ($n = 4$).

(<0.06 mg/kg) and Na (<6.8 mg/kg) were below the detection limits. The high contents of Fe, P, and Ca may be related to their initial concentrations that were the highest in the feedstock sludge (0.98, 1.4, and 0.69%, db, respectively). Many studies reported high concentrations of Fe (700–3000 ppm) in HTL biocrude from Fe-rich algae [80,82–85], while biocrude from other feedstocks (e.g., lignocellulose) could have lower Fe levels (100–300 ppm) [86,87]. Another study also reported comparable amounts of Zn (88.3 ppm) and Cr (6.6 ppm) in sludge-derived biocrude [5]. As previously mentioned, biocrude is required to be upgraded and refined to produce commercial fuels. However, metal contaminants in biocrude could lead to reactor plugging, catalysts fouling, and severe coking during the downstream upgrading process, e.g., hydrotreating [83]. It has been reported that Fe (>700 ppm) in algal-derived HTL biocrude caused plugging of catalyst beds after only 102 h of continuous hydroprocessing [85]. Abundant iron porphyrins (primarily N_4Fe_1) were identified in algal-derived biocrude. Another study also detected many iron porphyrins soluble in hemin-derived biocrude [82]. The iron porphyrins were found to have similar carbon number and double bond equivalent distributions to Ni and V porphyrins that were well-known in petroleum. Those metal porphyrins could degrade and deposit metal in the catalyst bed during hydrotreating as a result of hydrodemetallization reactions [85,88]. Seeing the considerable amount of Fe, Ni, and V in sludge-derived biocrude, pre-treatments, such as complete filtration [86], distillation [89], solvent extraction [90], and acid washing [87], are available and necessary for metal recycling and extending the bed lifetime of the hydrotreater.

3.4. *Plausible reaction pathway with in-situ catalysis*

The HTL reaction pathways for sludge are basically interactions between depolymerization and repolymerization of organic compounds. Initially, the large molecules, i.e., lipids, proteins, carbohydrates, and lignin/humic substances, are hydrolyzed into monomers. With increasing reaction temperature, those monomers undergo further decomposition or recombination reactions to form biocrude compounds. The potential biocrude-forming reaction network for HTL of sludge in Fig. 10 was proposed based on the current results and our previous literature reviews [13,14]. The chemical structures of main components identified by GC–MS were displayed.

Generally, lipids could be hydrolyzed to glycerol and long-chain fatty acids. Although cholesterol and its derivates (e.g., cholestene and cholestenone) have been previously identified from HTL of municipal sludge [91], digested sludge [92], and wastewater algae [51], its reaction pathway was not emphasized. The major presence of cholesterol derivates suggested that cholesterol-related reactions could be important pathways for HTL of feedstocks with cholesterol-rich lipids and thus were first highlighted in this study. Particularly, the increase of reaction temperature and residence time could promote the conversion of

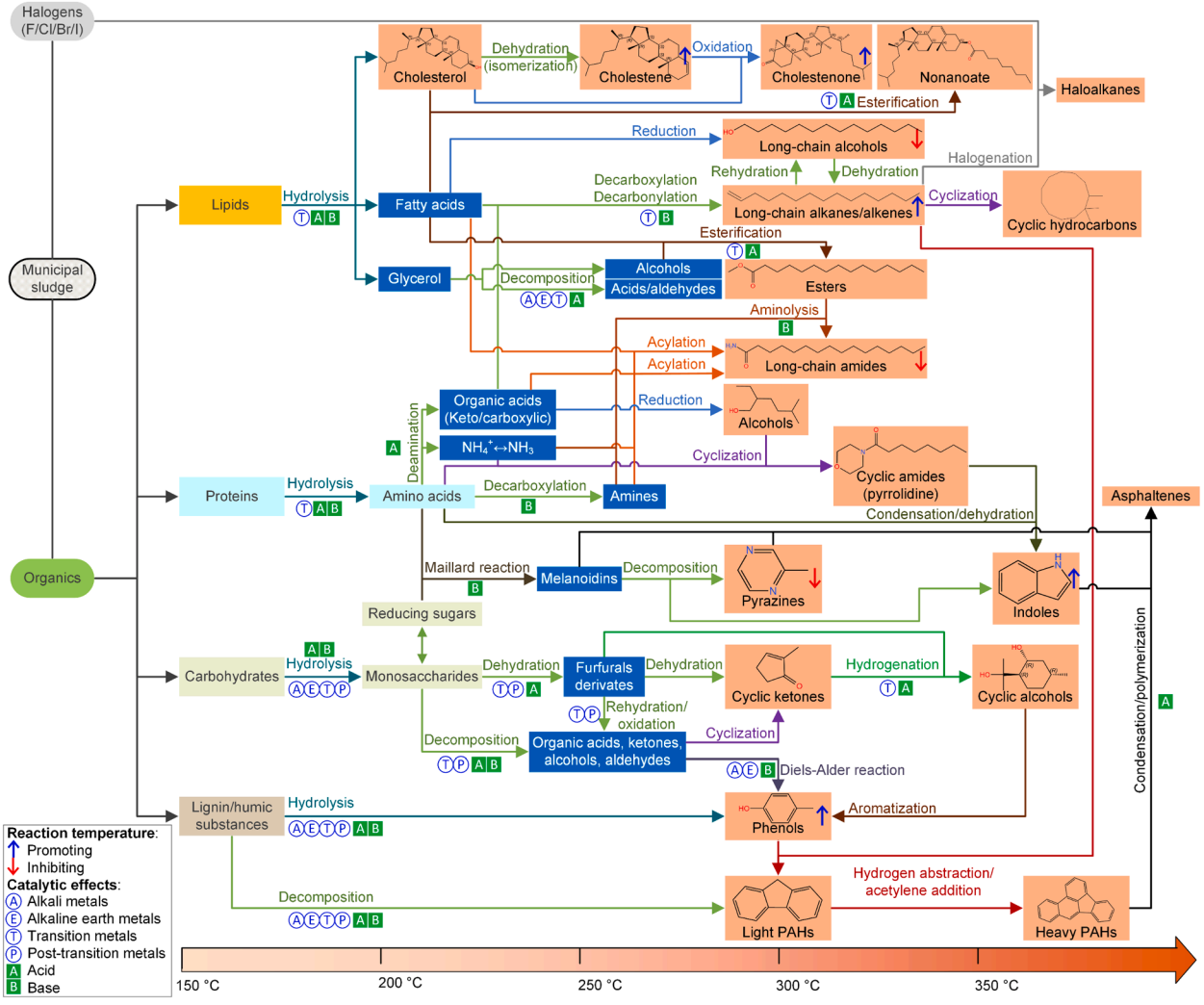

Fig. 10. Proposed biocrude-forming pathways for HTL of municipal sludge revealing effects of reaction temperature and catalysis by inherent metals and Brønsted sites.

cholesterol into cholestene and cholestenone. Fatty acids were found to have key contributions to producing biocrude by converting to long-chain alkenes, alcohols, esters, and amides. Higher temperatures also favored the formation of long-chain alkenes but reduced alcohols and amides due to enhanced decarboxylation and dehydration reactions. Proteins were hydrolyzed to amino acids, which could be further decomposed into short-chain acids, ammonia, and amines. Those intermediates were the main contributors to amides. Reducing sugars hydrolyzed from carbohydrates (e.g., cellulose and hemicellulose) could react with amino acids and generate N-heterocycles through Maillard reaction, which was found a major pathway due to the presence of abundant pyrazines. Increasing temperature could inhibit the Maillard reaction and decrease nitrogenous compounds. Monosaccharides from carbohydrates can form various intermediates, such as organic acids, alcohols, aldehydes, ketones, and furfural derivates, which would participate in other decomposition or recombination reactions. A few lignin and humic substances were mainly converted into aromatic compounds, such as phenols and polycyclic aromatic hydrocarbons (PAHs).

3.4.1. Catalytic effects from inherent metal groups

Considering the significant load of metals in feedstock sludge (0.18% alkali metals, 0.94% alkaline earth metals, 1.08% transition metals, and 0.27% post-transition metals on a dry basis), it is reasonable to infer that those inherent metals could have catalytic effects on the HTL reaction pathways. The use of metal catalysts in HTL has been widely reported [13,14]. The potential catalytic effects of metals on reaction pathways were summarized in Fig. 10. Compared to previous studies about HTL of municipal sludge [91,93], the contents of alkenes in biocrude were relatively high and acids were low in this study, which could be related to intrinsic transition metals in sludge, especially high content of Fe (0.98%, db). The catalytic effects of transition metals in HTL have been broadly reported. For example, dosing 0.25–1.25 g Fe_3O_4 catalyst in 33 mL of microalgae slurry during HTL could promote the transformation of acids to esters (reacting with alcohols) and olefin in biocrude; however, it may also enhance the formation of heterocyclic compounds due to improved decomposition of protein [94]. Such promotion from Fe could eventually improve biocrude yield, HHV, and energy recovery [95]. A similar report stated that transition metal (Co) could enhance the conversion of carbohydrates, and thus the obtained biocrude had high contents of hydrocarbons and low contents of acids [96]. Moreover, adding 0.025–0.5 g Zn^{2+} to 15 g of dry hyperaccumulator (*S. plumbizincicola*) was found to improve the hydrolysis of carbohydrates and lignin, catalyze the oxidation of furfurals derivates to acetic acid, decrease fatty acids, generate more aromatic compounds and light components, and promote deoxygenation reactions [97]. Most transition metals (Cr^{3+}, Co^{2+}, Cu^{2+}, Fe^{2+}, Fe^{3+}, Mn^{2+}, Ni^{2+}, and Zn^{2+}) were found to have similar catalytic effects in enhancing the hydrolysis of carbohydrates, dehydration of monosaccharides (e.g., xylose and glucose) to furfurals derivates, decomposition of monosaccharides into organic acids (e.g., lactic acid, levulinic acid, and formic acid), and conversion of heavy compounds to low-molecule-weight compounds in biocrude at an HTL temperature range of 155–330 °C [98–101]. However, the catalytic efficiency is related to the concentration and species of transition metals. In addition, transition metal sulfates showed higher catalytic activity than chloride and nitrate salts on glucose dehydration and rehydration to lactic acid at 155 °C [102]. They indicated that the complex of hydrated metal salts could bind with –OH groups of glucose through hydrogen bonding and promote the rapid conversion of α-anomers of glucose to β-anomers, and the catalytic efficiency also depended on the hydrogen bonding ability of associated anions (e.g., Cl^-, SO_4^{2-}, NO_3^-).

Post-transition metals (e.g., Al and Pb) were found to have similar catalytic effects to transition metals in terms of the hydrolysis of carbohydrates and the subsequent decomposition, dehydration, and rehydration reactions. Compared to Pb^{2+}, Al^{3+} (0.14 mmol) showed much higher efficiency in promoting the production of glucose and lactic acid from cellulose at 160–190 °C possibly due to its stronger Lewis acidity character [103]. Even a low Pb content (0–10 mmol/L) can promote the degradation of cellulose and lignin and catalyze the rehydration of 5-hydroxymethylfurfural (5-HMF) and produce more levulinic and formic acids at 180–270 °C [104]. The enhanced production of 5-HMF and furfural by $AlCl_3$ (0.01–0.03 M) was also observed for the hydrothermal conversion of poppy stalks at 180 °C [99].

Alkali and alkaline catalysts (e.g., carbonates and hydroxides) are commonly used to favor certain base-catalyzed condensation reactions by shifting ionic media, which can enhance the hydrolysis of carbohydrates and lignin and lead to aromatic oil formation [14,105]. However, the catalytic effects of alkali and alkaline earth metals themselves have been recognized. Alkali salt (NaCl) was found to catalyze the hydrolysis of sludge at 180–260 °C [106]. Adding Na^+, K^+, and Ca^{2+} at various pH (5–9) could strengthen the depolymerization of lignin and condensation of aromatic compounds during HTL (300 °C), especially at neutral pH [107]. Also, different alkali and alkaline hydroxides showed catalytic efficiencies for the hydrothermal decomposition of glycerol in sequence: KOH > NaOH > LiOH and $Ba(OH)_2$ > $Sr(OH)_2$ > $Ca(OH)_2$ > $Mg(OH)_2$ [108]. Alkaline catalysts could also neutralize the HTL reaction media and inhibit the repolymerization reactions of intermediates, which is probably responsible for the low distillation residue (Table 11) in biocrude from MS.

3.4.2. Catalytic effects from inherent Brønsted sites

The presence of abundant natural acids (e.g., volatile fatty acids) and high alkalinity in sludge (Table 1) brings another consideration of catalytic effects from Brønsted sites, i.e., acids (proton donor) and bases (proton acceptor). It is worth mentioning that many transition and post-transition metal ions (e.g., Fe^{3+}, Zn^{2+}, and Al^{3+}) can generate acid-base sites by forming complex ions with water, contributing to the synergistic effects on catalyst surfaces. Similarly, basic sites could also play important roles in the catalysis of alkali and alkaline earth metals. Both acidic and basic environments could promote hydrothermal reactions initially the breakage of macromolecules (e.g., hydrolysis), however, leading to different pathways [109]. Some generic pathways are summarized in Fig. 10. Carbohydrates are converted into 5-HMF and levulinic acids in acidic media, carboxylic acids under strong alkaline conditions, and their mixture in a neutral environment due to the self-ionization of H_2O to H^+ and OH^- during HTL [110,111]. Acidic conditions favor dehydration, deamination, and esterification and generate primarily oxygenates (e.g., carboxylic acids, ketones, and esters), while basic/alkaline media facilitate decarboxylation and aminolysis and produce hydrocarbon derivatives by reacting with organic acids [109,112]. Acids inhibit, but bases could promote the Maillard reaction [113]. Acidic environment could further advance condensation and repolymerization reactions of intermediates and decrease biocrude yield, whereas basic media prevent repolymerization [114]. Notably, many studies have demonstrated that adding external acids/bases/alkali salts has no significant effects on the yield and quality of biocrude generated from municipal sludge [13,14]. This could be attributed to the co-existence of abundant acidic-basic sites in original sludge.

In summary, increasing reaction temperature could improve the generation of hydrocarbons by promoting the deoxygenation and denitrification reactions during HTL, while the inherent metals and Brønsted sites in sludge would likely catalyze selected pathways and form major compounds. The proposed pathways are significant for guiding the production of high-quality biocrude. However, the understanding of metal catalysis is mainly limited to the hydrolysis of macromolecules and the decomposition of the corresponding monomers. Deeper perception of catalytic effects of metals should be exposed to turn high-load metals in sludge from burdens to benefits. Both acidic and basic Brønsted sites play vital roles in directing the reaction pathways while adjusting acid/base ratio might be a future focus to govern reaction pathways and produce high-quality biocrude [115].

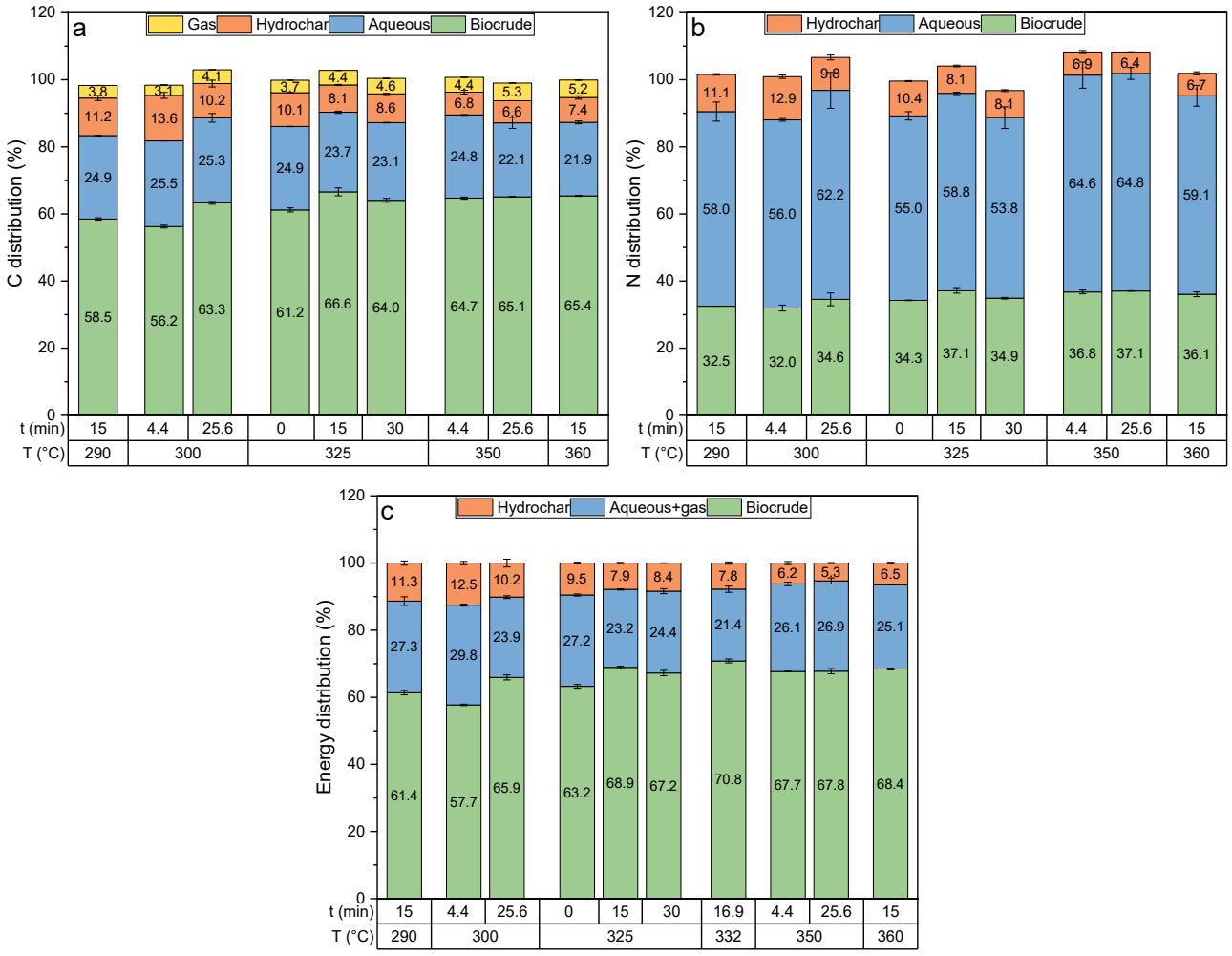

Fig. 11. Distribution of (a) carbon, (b) nitrogen, and (c) energy among HTL products on the mixed sludge input basis at various reaction temperatures (T) and residence time (t). The difference in energy distribution was attributed to aqueous + gas.

3.5. Elemental and energy distribution

3.5.1. CN and energy

The elemental and energy distribution was calculated based on the contents and yield of each product, which could be affected by the sludge compositions and HTL conditions. As shown in Fig. 11a, most C (56.2–66.6%) from the feedstock was recovered in biocrude, with the lowest observation at 300 °C and 4.4 min and the peak at the center point (325 °C and 15 min). Madsen and Glasius also recovered a comparable amount (42.7–70.2% of C) in biocrude from primary sludge at the temperature range of 250–350 °C and the response surface of CR was identical to biocrude yield and the findings of this study [19]. The highest CR in HTL aqueous (25.5%) was found at the lowest reaction severity (300 °C and 4.4 min), which gradually decreased with increasing reaction severity and reached the minimum of 21.9% at 360 °C and 15 min. CR in hydrochar varied at 6.6–13.6% and showed similar behaviors to that in HTL aqueous. Comparable C recoveries (15–29.6% in aqueous and 8.7–17.1% in hydrochar) and similar trends were also reported by a study for HTL (275–350 °C and 15–45 min) of algae grown from municipal wastewater [29]. On the contrary, C in gas form (3.1–5.3%) showed the opposite trend to HTL aqueous and hydrochar. It showed the minimum percentage at 300 °C and 4.4 min and the highest at 350 °C and 25.6 min. The low C loss (around 5%) as gas was also agreed by previous studies for HTL of primary and secondary sludge at 350 °C [2,116]. Nevertheless, C distributed in the aqueous phase was significant (>20%), which would require proper treatment and cost more. This highlights the importance of further recovery and promotes the valorization of HTL aqueous. Considering the existing facilities in WWTPs, coupling HTL and anaerobic digestion of aqueous could be a potential pathway, but additional investigations are needed. The benefits could be enhanced energy recovery and reduced effluent COD from HTL aqueous and subsequent aerobic treatment costs when returning to WWTPs.

The N distribution presented that most N (56–64.8%) from sludge feedstock was transferred to HTL aqueous (Fig. 11b). The N recovery (NR) in aqueous was found to enhance with reaction temperature. Another study also found > 60% of NR in HTL aqueous from municipal sludge at 180–300 °C for 30 min, which displayed positive relation to reaction temperature [53]. They also suggested that most protein-N in sludge was initially hydrolyzed and dissolved in HTL aqueous phase as organic-N (e.g., amino acids), which further decomposed and accumulated as NH_4^+–N. The NR in biocrude from mixed sludge was also high (32–37.1%). Notably, the NR in biocrude showed similar behaviors to its yield probably due to the consistent N contents (4.6–4.8%) in biocrude. Maillard reaction of amino-N and reducing sugar was mainly responsible for generating heterocyclic-N in biocrude [117]. The remaining NR in hydrochar was small (6.4–12.9%) and it was inversely proportional to reaction temperature and residence time. According to the mass balance, NR in the gas phase is negligible. It was reported that within a residence time of 1 h, NR in the gas phase was minimum or even negative but can suddenly reach > 20% after staying 2 h at 300 °C, possibly due to the accumulation of NH_3 and reduced soluble NH_3 in

aqueous [53]. The findings of this study were in agreement with a previous study for HTL of secondary sludge at 350 and 400 °C, which obtained 50–60%, 32–35%, 10–12%, and 0.4–0.8% of NR in aqueous, biocrude, hydrochar, and gas, respectively [116]. The high contents of N (7100–8867 mg/L total N) in HTL aqueous represent a great potential for nutrient recovery (e.g., ammonium sulfate and struvite). On the other hand, numerous studies have reported inhibition of anaerobic digestion activity by HTL aqueous due to high ammonia and abundant N-heterocycles (e.g., aziridines) [118]. This indicates that utilizing HTL aqueous by anaerobic digestion should be carefully examined.

Based on the energy distribution (Fig. 11c), most energy (57.7–70.8%) from sludge could be recovered as biocrude, whereas only 5.3–12.5% was converted to hydrochar. A similar ER in biocrude (67%) was also obtained from primary sludge at 340 °C for 20 min [119]. A continuous HTL system achieved up to 69.3% of biocrude ER from primary sludge at 325 °C for 9 min [11], which was close to this study. However, a supercritical condition (400 °C and 1 h) resulted in a lower ER (52%) in biocrude from municipal sludge [23]. The remaining energy in HTL aqueous and gas was relatively high (21.4–29.8%), but it was minimized at the optimized conditions (332 °C for 16.9 min). As HTL aqueous contained > 4 times CR higher than gas, it was believed that most of the remaining energy was stored in the aqueous. Using mixed model compounds (carbohydrate, protein, and lipid) for HTL at 300 and 350 °C, it was found that 44 and 59% of energy input were recovered in biocrude, respectively, while 17 and 11% energy could be recovered as methane by anaerobic digestion of HTL aqueous, respectively [120]. Many other studies also confirmed that HTL aqueous had a specific methane yield of 36–259 mL CH_4/g chemical oxygen demand [121–123]. Therefore, for its high potential, recovering the remaining energy from HTL aqueous is necessary, which can significantly improve the overall yield and sustainability of the holistic process. Meanwhile, energy in hydrochar could be used for combustion. Considering the low HHV (8–16 MJ/kg, db) and high ash contents (48–69%, db) in hydrochar (data not shown), further investigations and pretreatments are

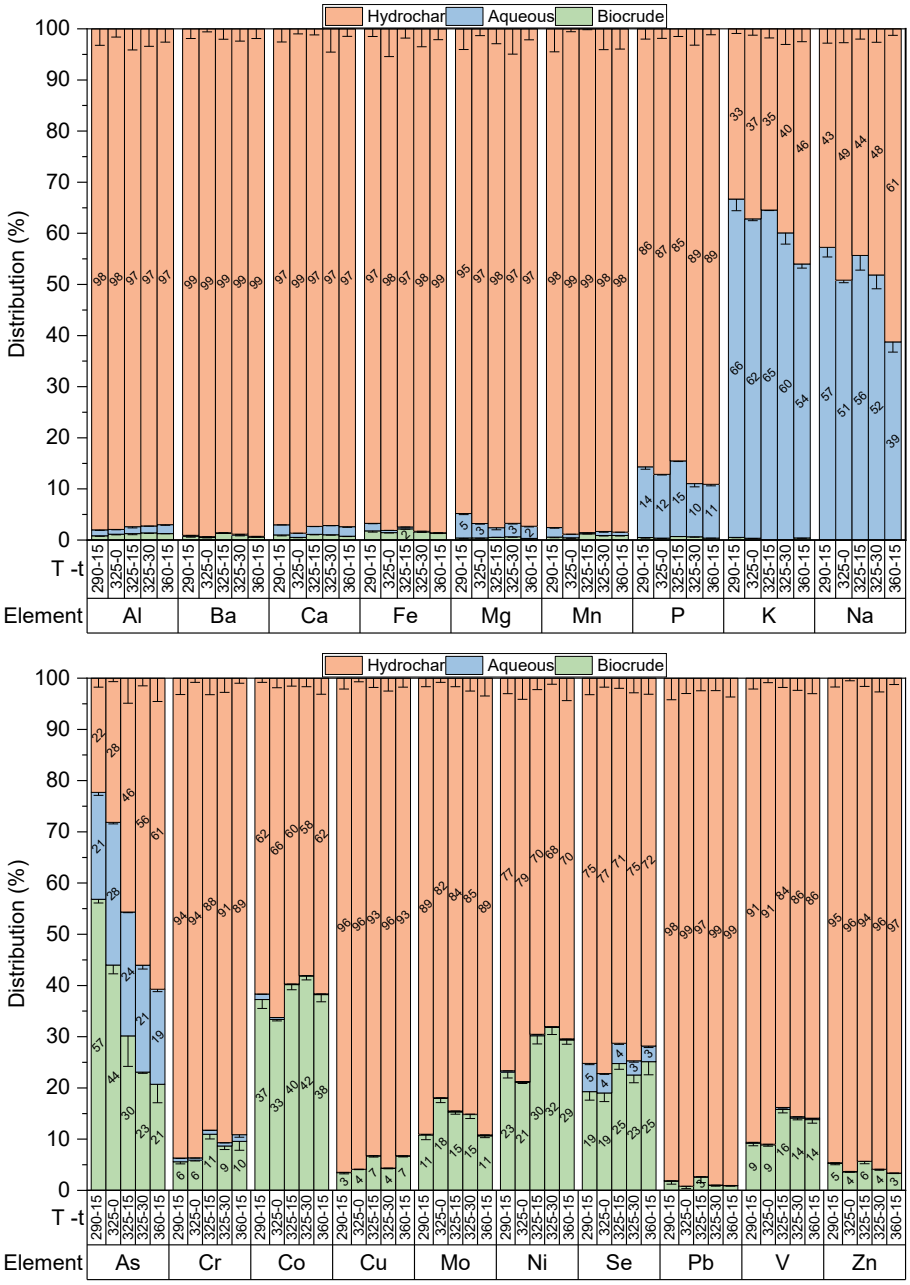

Fig. 12. Normalized distribution of inorganic elements among HTL products at various reaction temperatures (T, °C) and residence time (t, min).

needed to enhance its energy density and avoid possible ash slagging and fouling for combustion.

3.5.2. Inorganic elements

Abundant nutrient elements and heavy metals have been widely found in municipal sludge [13]. Those elements partition selectively among HTL biocrude, aqueous, and hydrochar. Discovering the partitioning behaviors of each element under various HTL conditions is essential to allow the control of unwanted elements (e.g., heavy metals) and recovery of desirable elements (e.g., nutrients). After HTL, the distribution of inorganic elements was determined by considering their concentrations and the weight of each product. As shown in Fig. 12, the elemental distribution was normalized based on the total amount of each element recovered in each product. Most of the examined elements were distributed in hydrochar with > 60% of the total. In particular, alkaline earth metals (e.g., Mg, Ca, and Ba), Al, Fe, Mn and were predominantly (>95%) present in hydrochar, probably due to their affinity to P that formed phosphate precipitates [3]. >85% P was converted into hydrochar with a concentration up to 855 mg/g, providing great potential for P recovery. On the other hand, the large fraction (>60%) of potential contaminants of concerns (e.g., Cr, Co, Cu, Mo, Ni, Se, Pb, and Zn) in hydrochar could be problematic during P extraction and thus require attention.

A large portion of alkali metals, such as K (45–56%) and Na (28–47%), were released in the HTL aqueous, but their amount gradually decreased with increasing reaction severity, which transferred to hydrochar. [80] also found that K and Na were mostly present in HTL aqueous and their percentages reduced after some time. Unlike other elements with negligible allocations (<2%), many transition metals, such as Co (33–42%), Ni (21–32%), Mo (11–18%), V (9–16%), Cr (6–11%), Cu (3–7%), and Zn (3–5%), plus metalloids As (21–57%) and Se (19–25%) were dispersed to biocrude in a considerable level. Although Fe had the highest concentration in biocrude compared to other metals, <2% of the feedstock resided in biocrude. When upgrading biocrude, attention should be paid to those inorganics, especially Ni and V, for their deactivation effects on catalysts [83]. The migration of As, Cr, Cu, Ni, and Zn into biocrude from HTL of various manures and municipal sludge has also been reported by many other studies [124–126]. Compared to other heavy metals, metalloid As exhibited a unique distribution behavior, which was mainly dispersed to biocrude, followed by hydrochar (22–61%) and HTL aqueous (19–28%). In general, its percentage was reduced in biocrude and aqueous but increased in hydrochar with intensifying reaction severity. The high mobility of As during HTL has been widely reported [127]. Arsenate (V) and dimethylarsinic acid were found the main species in secondary sludge at pH < 6.5 [128]. It was suggested that As(V) in feedstocks could be converted into more soluble As(III) [81], while arsenate with other metals was precipitated in hydrochar and As in organic form (e.g., roxarsone) probably contributed to solvent-extracted biocrude [126]. Immobilization of As during HTL is worthy of investigation. Higher reaction severities (i.e., higher temperature and/or longer residence time) could cause more Cr, Ni, Se, and V transferring to biocrude from hydrochar, while other elements did not show noticeable changes in terms of reaction temperature and residence time. It was also reported that supercritical conditions (e.g., 400 °C) may significantly enhance the mobility of inorganic elements (e.g., Cu, Fe, K, and Zn) [116]. In summary, most nutrients and heavy metals were accumulated in hydrochar, giving both opportunities for recovery and challenges for separation; many metals were well dispersed to biocrude, indicating the necessity of monitoring and pretreatments for upgrading. Revealing the fate of inorganic elements is essential for guiding the downstream utilization and treatment of HTL products.

4. Conclusion

The biocrude production and ER from HTL of municipal mixed sludge were investigated using RSM. Various reaction temperatures and residence time were examined to explore their effects on ER, elemental distribution, and biocrude characteristics. The major conclusions were drawn as follows:

- Through modeling and optimization, maximum biocrude yield (48.9%, daf), CR (68.6%), and ER (70.8%) could be achieved in the same HTL operating conditions (332 °C for 16.9 min). Meanwhile, the generation of by-products (i.e., aqueous, hydrochar, and gas) could be minimized. A high EROI (2.42) was also achieved.
- HTL reaction temperature and residence time showed positive effects on biocrude C content and HHV but negatively affected biocrude O content and O/C. Higher reaction severities could also reduce biocrude TAN, thus enhancing the quality. The batch reactor could generate biocrude with similar properties (e.g., CHNSO, HHV, and TAN) to those from plug-flow continuous systems.
- GC–MS indicated that increasing reaction temperature significantly reduced nitrogenous compounds in biocrude by inhibiting the formation of N-heterocycles and amides and generating more hydrocarbons. Cholesterol-related reactions were important pathways for biocrude formation from sludge and were highlighted for the first time. Inherent metals and Brønsted sites in sludge could play catalytic roles in HTL reaction pathways. DTG-DSC analysis suggested the presence of resins and asphaltenes in biocrude.
- Sludge-derived biocrude contained trace amounts of metal contaminants, especially Fe (497–656 mg/kg), which can be separated and recycled prior to the downstream upgrading process. Higher reaction temperature decreased the concentrations of Zn, K, and As but enhanced Cu, Ni, Cr, and V, while longer residence time reduced As but increased Ca, Ni, Cr, Ba, Mn, Co, and V in biocrude.
- After HTL, most energy and C were recovered as biocrude, while the majority N (53–65%) was distributed in aqueous, and most P (85–89%) was concentrated in hydrochar. This implies that HTL of municipal sludge represents a justifiable process to allow resource recovery from each product stream. Most heavy metals were accumulated in hydrochar, so their separation from P will be of particular interest for P recovery.
- Overall, increasing reaction temperature and/or residence time could improve biocrude quality but decrease the ER and/or EROI. Through RSM optimization, the balance between quality and ER could be obtained.

Declaration of Competing Interest

The authors declare that they have no known competing financial interests or personal relationships that could have appeared to influence the work reported in this paper.

Data availability

Data will be made available on request.

Acknowledgements

This research was funded by the Natural Sciences and Engineering Research Council of Canada (NSERC) and Metro Vancouver Industrial Research Chair Program in Advanced Resource Recovery from Wastewater (IRCPJ 548816-18). This study was also supported by the NSERC Canada Graduate Scholarship – Doctoral program. The authors are

grateful to the anonymous reviewers for their insightful suggestions and contribution to the improvement of this article.

Appendix A. Supplementary data

Supplementary data to this article can be found online at https://doi.org/10.1016/j.cej.2022.137838.

References

[1] CCME, Canada-wide approach for the management of wastewater biosolids, 2012. publications.gc.ca/pub?id=9.697780&sl=1 (accessed August 15, 2020).

[2] P.A. Marrone, D.C. Elliott, J.M. Billing, R.T. Hallen, T.R. Hart, P. Kadota, J. C. Moeller, M.A. Randel, A.J. Schmidt, Bench-scale evaluation of hydrothermal processing technology for conversion of wastewater solids to fuels, Water Environ. Res. 90 (2018) 329–342, https://doi.org/10.2175/106143017x15131012152861.

[3] H. Liu, G. Hu, I.A. Basar, J. Li, N. Lyczko, A. Nzihou, C. Eskicioglu, Phosphorus recovery from municipal sludge-derived ash and hydrochar through wet-chemical technology: A review towards sustainable waste management, Chem. Eng. J. 417 (2021), 129300, https://doi.org/10.1016/j.cej.2021.129300.

[4] G. Kor-Bicakci, C. Eskicioglu, Recent developments on thermal municipal sludge pretreatment technologies for enhanced anaerobic digestion, Renew. Sustain. Energy Rev. 110 (2019) 423–443, https://doi.org/10.1016/j.rser.2019.05.002.

[5] D. Xu, G. Lin, L. Liu, Y. Wang, Z. Jing, S. Wang, Comprehensive evaluation on product characteristics of fast hydrothermal liquefaction of sewage sludge at different temperatures, Energy. 159 (2018) 686–695, https://doi.org/10.1016/j.energy.2018.06.191.

[6] S. Donatello, C.R. Cheeseman, Recycling and recovery routes for incinerated sewage sludge ash (ISSA): A review, Waste Manag. 33 (2013) 2328–2340, https://doi.org/10.1016/j.wasman.2013.05.024.

[7] H.-J. Huang, Y.-C. Chang, F.-Y. Lai, C.-F. Zhou, Z.-Q. Pan, X.-F. Xiao, J.-X. Wang, C.-H. Zhou, Co-liquefaction of sewage sludge and rice straw/wood sawdust: The effect of process parameters on the yields/properties of bio-oil and biochar products, Energy. 173 (2019) 140–150.

[8] Y. Kim, W. Parker, A technical and economic evaluation of the pyrolysis of sewage sludge for the production of bio-oil, Bioresour. Technol. 99 (2008) 1409–1416, https://doi.org/10.1016/j.biortech.2007.01.056.

[9] T. Mathimani, N. Mallick, A review on the hydrothermal processing of microalgal biomass to bio-oil - Knowledge gaps and recent advances, J. Clean. Prod. 217 (2019) 69–84, https://doi.org/10.1016/j.jclepro.2019.01.129.

[10] C. vom Eyser, K. Palmu, T.C. Schmidt, J. Tuerk, Pharmaceutical load in sewage sludge and biochar produced by hydrothermal carbonization, Sci. Total Environ. 537 (2015) 180–186, https://doi.org/10.1016/j.scitotenv.2015.08.021.

[11] L.B. Silva Thomsen, P.N. Carvalho, J.S. dos Passos, K. Anastasakis, K. Bester, P. Biller, Hydrothermal liquefaction of sewage sludge; energy considerations and fate of micropollutants during pilot scale processing, Water Res. 183 (2020), 116101, https://doi.org/10.1016/j.watres.2020.116101.

[12] A.V. Mitroshkov, L. Zhong, L.M.P. Thomas, Analysis of Perfluorinated, Pharmaceutical, Personal Care Compounds and Heavy Metals in Waste Water Sludge using GC-MS/MS and Multicollector ICP-MS, U.S. Department of Energy, Richland, WA (United States) (2019), https://doi.org/10.2172/1494304.

[13] H. Liu, I.A. Basar, A. Nzihou, C. Eskicioglu, Hydrochar derived from municipal sludge through hydrothermal processing: A critical review on its formation, characterization, and valorization, Water Res. 199 (2021), 117186, https://doi.org/10.1016/j.watres.2021.117186.

[14] I.A. Basar, H. Liu, H. Carrere, E. Trably, C. Eskicioglu, A review on key design and operational parameters to optimize and develop hydrothermal liquefaction of biomass for biorefinery applications, Green Chem. 23 (2021) 1404–1446, https://doi.org/10.1039/D0GC04092D.

[15] P. Biller, A.B. Ross, Potential yields and properties of oil from the hydrothermal liquefaction of microalgae with different biochemical content, Bioresour. Technol. 102 (2011) 215–225, https://doi.org/10.1016/j.biortech.2010.06.028.

[16] J. Lu, Z. Liu, Y. Zhang, P.E. Savage, Synergistic and Antagonistic Interactions during Hydrothermal Liquefaction of Soybean Oil, Soy Protein, Cellulose, Xylose, and Lignin, ACS Sustain. Chem. Eng. 6 (2018) 14501–14509, https://doi.org/10.1021/acssuschemeng.8b03156.

[17] J. Yang, Q.(. He, H. Niu, K. Corscadden, T. Astatkie, Hydrothermal liquefaction of biomass model components for product yield prediction and reaction pathways exploration, Appl. Energy 228 (2018) 1618–1628.

[18] S. Mahadevan Subramanya, P.E. Savage, Identifying and Modeling Interactions between Biomass Components during Hydrothermal Liquefaction in Sub-, Near-, and Supercritical Water, ACS Sustain, Chem. Eng. 9 (2021) 13874–13882, https://doi.org/10.1021/acssuschemeng.1c04810.

[19] R.B. Madsen, M. Glasius, How Do Hydrothermal Liquefaction Conditions and Feedstock Type Influence Product Distribution and Elemental Composition? Ind. Eng. Chem. Res. 58 (2019) 17583–17600, https://doi.org/10.1021/acs.iecr.9b02337.

[20] L. Nazari, Z. Yuan, M.B. Ray, C. (Charles) Xu, Co-conversion of waste activated sludge and sawdust through hydrothermal liquefaction: Optimization of reaction parameters using response surface methodology, Appl. Energy. 203 (2017) 1–10, https://doi.org/10.1016/j.apenergy.2017.06.009.

[21] J.L. Faeth, P.J. Valdez, P.E. Savage, Fast hydrothermal liquefaction of nannochloropsis sp. to produce biocrude, Energy Fuels 27 (2013) 1391–1398, https://doi.org/10.1021/ef301925d.

[22] A. Gollakota, P.E. Savage, Biocrude Production from Fast and Isothermal Hydrothermal Liquefaction of Chitin, Energy Fuels 33 (2019) 11328–11338, https://doi.org/10.1021/acs.energyfuels.9b03209.

[23] L. Qian, S. Wang, P.E. Savage, Hydrothermal liquefaction of sewage sludge under isothermal and fast conditions, Bioresour. Technol. 232 (2017) 27–34, https://doi.org/10.1016/j.biortech.2017.02.017.

[24] P. Das, S. Khan, M. AbdulQuadir, M. Thaher, M. Waqas, A. Easa, E.S.M. Attia, H. Al-Jabri, Energy recovery and nutrients recycling from municipal sewage sludge, Sci. Total Environ. 715 (2020), 136775, https://doi.org/10.1016/j.scitotenv.2020.136775.

[25] S.K. Bauer, C.F. Reynolds, S. Peng, L.M. Colosi, Evaluating the Water Quality Impacts of Hydrothermal Liquefaction Assessment of Carbon, Nitrogen, and Energy Recovery, Bioresour. Technol. Reports. 2 (2018) 115–120, https://doi.org/10.1016/j.biteb.2018.04.010.

[26] İ.A. Başar, N.A. Perendeci, Optimization of zero-waste hydrogen peroxide - Acetic acid pretreatment for sequential ethanol and methane production, Energy. 225 (2021), 120324, https://doi.org/10.1016/j.energy.2021.120324.

[27] C. Hong, Z. Wang, Y. Si, Z. Li, Y. Xing, J. Hu, Y. Li, Preparation of bio-oils by hydrothermal liquefaction (HTL) of penicillin fermentation residue (PR): Optimization of conditions and mechanistic studies, Sci. Total Environ. 761 (2021), 143216, https://doi.org/10.1016/j.scitotenv.2020.143216.

[28] Y. Chang, X.-F. Xiao, H. Huang, Y.-D. Xiao, H.-S. Fang, J.-B. He, C.-H. Zhou, Transformation characteristics of polycyclic aromatic hydrocarbons during hydrothermal liquefaction of sewage sludge, J. Supercrit. Fluids 170 (2021), 105158, https://doi.org/10.1016/j.supflu.2020.105158.

[29] E.A. Couto, F. Pinto, F. Varela, A. Reis, P. Costa, M.L. Calijuri, Hydrothermal liquefaction of biomass produced from domestic sewage treatment in high-rate ponds, Renew. Energy. 118 (2018) 644–653, https://doi.org/10.1016/j.renene.2017.11.041.

[30] Y. Fan, F.G. Fonseca, M. Gong, A. Hoffmann, U. Hornung, N. Dahmen, Energy valorization of integrating lipid extraction and hydrothermal liquefaction of lipid-extracted sewage sludge, J. Clean. Prod. 285 (2021), 124895, https://doi.org/10.1016/j.jclepro.2020.124895.

[31] S. Inoue, S. Sawayama, Y. Dote, T. Ogi, Behaviour of nitrogen during liquefaction of dewatered sewage sludge, Biomass Bioenergy 12 (1997) 473–475, https://doi.org/10.1016/S0961-9534(97)00017-2.

[32] K. Kapusta, Effect of ultrasound pretreatment of municipal sewage sludge on characteristics of bio-oil from hydrothermal liquefaction process, Waste Manag. 78 (2018) 183–190, https://doi.org/10.1016/j.wasman.2018.05.043.

[33] S. Mishra, K. Mohanty, Co-HTL of domestic sewage sludge and wastewater treatment derived microalgal biomass – An integrated biorefinery approach for sustainable biocrude production, Energy Convers. Manag. 204 (2020), 112312, https://doi.org/10.1016/j.enconman.2019.112312.

[34] L. Qian, S. Wang, P.E. Savage, Fast and isothermal hydrothermal liquefaction of sludge at different severities: Reaction products, pathways, and kinetics, Appl. Energy 260 (2020), 114312, https://doi.org/10.1016/j.apenergy.2019.114312.

[35] B. Wu, S.M. Berg, C.K. Remucal, T.J. Strathmann, Evolution of N-Containing Compounds during Hydrothermal Liquefaction of Sewage Sludge, ACS Sustain. Chem. Eng. 8 (2020) 18303–18313, https://doi.org/10.1021/acssuschemeng.0c07060.

[36] Y.H. Kuan, F.H. Wu, G.B. Chen, H.T. Lin, T.H. Lin, Study of the combustion characteristics of sewage sludge pyrolysis oil, heavy fuel oil, and their blends, Energy. 201 (2020), 117559, https://doi.org/10.1016/j.energy.2020.117559.

[37] J.M. Jarvis, J.M. Billing, R.T. Hallen, A.J. Schmidt, T.M. Schaub, Hydrothermal Liquefaction Biocrude Compositions Compared to Petroleum Crude and Shale Oil, Energy Fuels 31 (2017) 2896–2906, https://doi.org/10.1021/acs.energyfuels.6b03022.

[38] A. Ali Shah, S. Sohail Toor, T. Hussain Seehar, K.K. Sadetmahaleh, T. Helmer Pedersen, A. Haaning Nielsen, L. Aistrup Rosendahl, Aistrup Rosendahl, Bio-crude production through co-hydrothermal processing of swine manure with sewage sludge to enhance pumpability, Fuel 288 (2021) 119407.

[39] C. Gai, Y. Zhang, W.T. Chen, P. Zhang, Y. Dong, Energy and nutrient recovery efficiencies in biocrude oil produced via hydrothermal liquefaction of Chlorella pyrenoidosa, RSC Adv. 4 (2014) 16958–16967, https://doi.org/10.1039/c3ra46607h.

[40] C. Prestigiacomo, P. Costa, F. Pinto, B. Schiavo, A. Siragusa, O. Scialdone, A. Galia, Sewage sludge as cheap alternative to microalgae as feedstock of catalytic hydrothermal liquefaction processes, J. Supercrit. Fluids 143 (2019) 251–258, https://doi.org/10.1016/j.supflu.2018.08.019.

[41] H. Sudibyo, K. Wang, J.W. Tester, Hydrothermal Liquefaction of Acid Whey: Effect of Feedstock Properties and Process Conditions on Energy and Nutrient Recovery, ACS Sustain. Chem. Eng. 9 (2021) 11403–11415, https://doi.org/10.1021/acssuschemeng.1c03358.

[42] P.A. Marrone, Genifuel Hydrothermal Processing Bench-Scale Technology Evaluation Project, Alexandria, VA, 2016. https://www.iwapublishing.com/books/genifuel-hydrothermal-processing-bench-scale-technology-evaluation-report.

[43] K. Anastasakis, P. Biller, R.B. Madsen, M. Glasius, I. Johannsen, Continuous Hydrothermal Liquefaction of Biomass in a Novel Pilot Plant with Heat Recovery and Hydraulic Oscillation, Energies 11 (2018) 1–23, https://doi.org/10.3390/en11102695.

[44] R. Liu, W. Tian, S. Kong, Y. Meng, H. Wang, J. Zhang, Effects of inorganic and organic acid pretreatments on the hydrothermal liquefaction of municipal

secondary sludge, Energy Convers. Manage. 174 (2018) 661–667, https://doi.org/10.1016/j.enconman.2018.08.058.
[45] R. Shakya, S. Adhikari, R. Mahadevan, S.R. Shanmugam, H. Nam, E.B. Hassan, T. A. Dempster, Influence of biochemical composition during hydrothermal liquefaction of algae on product yields and fuel properties, Bioresour. Technol. 243 (2017) 1112–1120, https://doi.org/10.1016/j.biortech.2017.07.046.
[46] J.H. Lee, H. Hwang, J. Moon, J.W. Choi, Characterization of hydrothermal liquefaction products from coconut shell in the presence of selected transition metal chlorides, J. Anal. Appl. Pyrol. 122 (2016) 415–421, https://doi.org/10.1016/j.jaap.2016.11.005.
[47] R. Shakya, J. Whelen, S. Adhikari, R. Mahadevan, S. Neupane, Effect of temperature and Na2CO3 catalyst on hydrothermal liquefaction of algae, Algal Res. 12 (2015) 80–90, https://doi.org/10.1016/j.algal.2015.08.006.
[48] R. Mujahid, A. Riaz, R. Insyani, J. Kim, A centrifugation-first approach for recovering high-yield bio-oil with high calorific values in biomass liquefaction: A case study of sewage sludge, Fuel 262 (2020), 116628, https://doi.org/10.1016/j.fuel.2019.116628.
[49] G. Haarlemmer, C. Guizani, S. Anouti, M. Déniel, A. Roubaud, S. Valin, Analysis and comparison of bio-oils obtained by hydrothermal liquefaction and fast pyrolysis of beech wood, Fuel 174 (2016) 180–188, https://doi.org/10.1016/j.fuel.2016.01.082.
[50] W.T. Chen, Y. Zhang, T.H. Lee, Z. Wu, B. Si, C.F.F. Lee, A. Lin, B.K. Sharma, Renewable diesel blendstocks produced by hydrothermal liquefaction of wet biowaste, Nat. Sustain. 1 (2018) 702–710, https://doi.org/10.1038/s41893-018-0172-3.
[51] R.B. Carpio, Y. Zhang, C.T. Kuo, W.T. Chen, L.C. Schideman, R. de Leon, Effects of reaction temperature and reaction time on the hydrothermal liquefaction of demineralized wastewater algal biomass, Bioresour. Technol. Reports. 14 (2021), 100679, https://doi.org/10.1016/j.biteb.2021.100679.
[52] W.T. Chen, Y. Zhang, J. Zhang, G. Yu, L.C. Schideman, P. Zhang, M. Minarick, Hydrothermal liquefaction of mixed-culture algal biomass from wastewater treatment system into bio-crude oil, Bioresour. Technol. 152 (2014) 130–139, https://doi.org/10.1016/j.biortech.2013.10.111.
[53] X. Zhuang, Y. Huang, Y. Song, H. Zhan, X. Yin, C. Wu, The transformation pathways of nitrogen in sewage sludge during hydrothermal treatment, Bioresour. Technol. 245 (2017) 463–470, https://doi.org/10.1016/j.biortech.2017.08.195.
[54] S. He, M. Zhao, J. Wang, Z. Cheng, B. Yan, G. Chen, Hydrothermal liquefaction of low-lipid algae Nannochloropsis sp. and Sargassum sp.: Effect of feedstock composition and temperature, Sci. Total Environ. 712 (2020), 135677, https://doi.org/10.1016/j.scitotenv.2019.135677.
[55] J. Zimmermann, K. Raffelt, N. Dahmen, Sequential Hydrothermal Processing of Sewage Sludge to Produce Low Nitrogen Biocrude, Processes. 9 (2021) 491, https://doi.org/10.3390/pr9030491.
[56] R. Li, W. Teng, Y. Li, E. Liu, Liquefaction of Sewage Sludge to Produce Bio-oil in Different Organic Solvents with in Situ Hydrogenation, Energy Fuels 33 (2019) 7415–7423, https://doi.org/10.1021/acs.energyfuels.9b01434.
[57] M. Wądrzyk, R. Janus, M.P. Vos, D.W.F. Brilman, Effect of process conditions on bio-oil obtained through continuous hydrothermal liquefaction of Scenedesmus sp. microalgae, J. Anal. Appl. Pyrol. 134 (2018) 415–426, https://doi.org/10.1016/j.jaap.2018.07.008.
[58] H.-J. Huang, X.-Z. Yuan, H.-n. Zhu, H. Li, Y. Liu, X.-l. Wang, G.-M. Zeng, Comparative studies of thermochemical liquefaction characteristics of microalgae, lignocellulosic biomass and sewage sludge, Energy. 56 (2013) 52–60.
[59] W. Yang, X. Li, Z. Li, C. Tong, L. Feng, Understanding low-lipid algae hydrothermal liquefaction characteristics and pathways through hydrothermal liquefaction of algal major components: Crude polysaccharides, crude proteins and their binary mixtures, Bioresour. Technol. 196 (2015) 99–108, https://doi.org/10.1016/j.biortech.2015.07.020.
[60] Y. Fan, U. Hornung, K. Raffelt, N. Dahmen, The influence of lipids on the fate of nitrogen during hydrothermal liquefaction of protein-containing biomass, J. Anal. Appl. Pyrol. 147 (2020), 104798, https://doi.org/10.1016/j.jaap.2020.104798.
[61] Y. Qiu, A. Aierzhati, J. Cheng, H. Guo, W. Yang, Y. Zhang, Biocrude Oil Production through the Maillard Reaction between Leucine and Glucose during Hydrothermal Liquefaction, Energy Fuels 33 (2019) 8758–8765, https://doi.org/10.1021/acs.energyfuels.9b01875.
[62] D.C. Hietala, P.E. Savage, Reaction pathways and kinetics of cholesterol in high-temperature water, Chem. Eng. J. 265 (2015) 129–137, https://doi.org/10.1016/j.cej.2014.12.020.
[63] L. Li, X. Yin, C. Wu, L. Ma, Z. Zhou, Kinetic studies on the pyrolysis and combustion of bio-oil, in: ISES Sol. World Congr. 2007, ISES 2007, 2007: pp. 2393–2396. doi:10.1007/978-3-540-75997-3_483.
[64] M. Ahmadi Khoshooei, F. Fazlollahi, Y. Maham, A. Hassan, P. Pereira-Almao, A review on the application of differential scanning calorimetry (DSC) to petroleum products: Wax crystallization study and structural analysis, J. Therm. Anal. Calorim. 138 (2019) 3485–3510, https://doi.org/10.1007/s10973-019-08022-0.
[65] S. Xiu, H.K. Rojanala, A. Shahbazi, E.H. Fini, L. Wang, Pyrolysis and combustion characteristics of Bio-oil from swine manure, J. Therm. Anal. Calorim. 107 (2012) 823–829, https://doi.org/10.1007/s10973-011-1604-8.
[66] Y. Wang, S. Ren, L. Zhang, J. Deng, X. Peng, H. Cheng, New insights into the oxidation behaviors of crude oils and their exothermic characteristics: Experimental study via simultaneous TGA/DSC, Fuel 219 (2018) 141–150, https://doi.org/10.1016/j.fuel.2018.01.076.
[67] M.V. Kök, O. Karacan, Pyrolysis analysis and kinetics of crude oils, J. Therm. Anal. Calorim. 52 (1998) 781–788, https://doi.org/10.1023/A:1010114624345.
[68] W.H. Chen, Y.Y. Lin, H.C. Liu, T.C. Chen, C.H. Hung, C.H. Chen, H.C. Ong, A comprehensive analysis of food waste derived liquefaction bio-oil properties for industrial application, Appl. Energy 237 (2019) 283–291, https://doi.org/10.1016/j.apenergy.2018.12.084.
[69] M.V. Kök, O. Karacan, Pyrolysis Analysis of Crude Oils and Their Fractions, Energy Fuels 11 (1997) 385–391, https://doi.org/10.1021/ef960162+.
[70] S. Zhao, W. Pu, M.A. Varfolomeev, Y. Liu, Z. Liu, Oxidation characteristics of heavy oil and its SARA fractions during combustion using TG-FTIR, J. Pet. Sci. Eng. 192 (2020), 107331, https://doi.org/10.1016/j.petrol.2020.107331.
[71] S. Zhao, W. Pu, B. Sun, F. Gu, L. Wang, Comparative evaluation on the thermal behaviors and kinetics of combustion of heavy crude oil and its SARA fractions, Fuel 239 (2019) 117–125, https://doi.org/10.1016/j.fuel.2018.11.014.
[72] M.V. Kok, A.S. Gundogar, DSC study on combustion and pyrolysis behaviors of Turkish crude oils, Fuel Process. Technol. 116 (2013) 110–115, https://doi.org/10.1016/j.fuproc.2013.05.001.
[73] S. Chiaberge, A. Siviero, C. Passerini, S. Pavoni, D. Bianchi, M.S. Haider, D. Castello, Co-processing of Hydrothermal Liquefaction Sewage Sludge Biocrude with a Fossil Crude Oil by Codistillation: A Detailed Characterization Study by FTICR Mass Spectrometry, Energy Fuels 35 (2021) 13830–13839, https://doi.org/10.1021/acs.energyfuels.1c01673.
[74] G. Robertson, K.V. Adiningtyas, S.A. Ebrahim, L. Scoles, E.A. Baranova, D. Singh, Understanding the nature of bio-asphaltenes produced during hydrothermal liquefaction, Renew. Energy. 173 (2021) 128–140, https://doi.org/10.1016/j.renene.2021.03.099.
[75] M. Jin, Y.K. Oh, Y.K. Chang, M. Choi, Optimum Utilization of Biochemical Components in Chlorella sp. KR1 via Subcritical Hydrothermal Liquefaction, ACS Sustain, Chem. Eng. 5 (2017) 7240–7248, https://doi.org/10.1021/acssuschemeng.7b01473.
[76] B. Adnadjevic, A. Popovic, Hydrothermal transformation of sawdust into synthetic coke-mechanism and influence of experimental parameters, Energy Sources, Part A Recover. Util. Environ. Eff. 31 (2009) 807–813, https://doi.org/10.1080/15567030701752750.
[77] S. Zhao, W. Pu, X. Peng, J. Zhang, H. Ren, Low-temperature oxidation of heavy crude oil characterized by TG, DSC, GC-MS, and negative ion ESI FT-ICR MS, Energy 214 (2021), 119004, https://doi.org/10.1016/j.energy.2020.119004.
[78] M.V. Kök, K.G. Gul, Combustion characteristics and kinetic analysis of Turkish crude oils and their SARA fractions by DSC, J. Therm. Anal. Calorim. 114 (2013) 269–275, https://doi.org/10.1007/s10973-013-3256-3.
[79] Y.L. Shishkin, A new quick method of determining the group hydrocarbon composition of crude oils and oil heavy residues based on their oxidative distillation (cracking) as monitored by differential scanning calorimetry and thermogravimetry, Thermochim Acta 440 (2006) 156–165, https://doi.org/10.1016/j.tca.2005.11.008.
[80] J. Jiang, P.E. Savage, Metals and Other Elements in Biocrude from Fast and Isothermal Hydrothermal Liquefaction of Microalgae, Energy Fuels 32 (2018) 4118–4126, https://doi.org/10.1021/acs.energyfuels.7b03144.
[81] H. Li, M. Cao, Y. Zhang, Z. Liu, Hydrothermal liquefaction accelerates the toxicity and solubility of arsenic in biowaste, J. Hazard. Mater. 418 (2021), 126341, https://doi.org/10.1016/j.jhazmat.2021.126341.
[82] J. Jiang, J.J. Serago, K. Torres, E. Rapp, P.E. Savage, Fate of iron during hydrothermal liquefaction of hemin, J. Supercrit. Fluids 157 (2020), 104705, https://doi.org/10.1016/j.supflu.2019.104705.
[83] M.S. Haider, D. Castello, L.A. Rosendahl, The Art of Smooth Continuous Hydroprocessing of Biocrudes Obtained from Hydrothermal Liquefaction: Hydrodemetallization and Propensity for Coke Formation, Energy Fuels 35 (2021) 10611–10622, https://doi.org/10.1021/acs.energyfuels.1c01228.
[84] J. Jiang, P.E. Savage, Influence of process conditions and interventions on metals content in biocrude from hydrothermal liquefaction of microalgae, Algal Res. 26 (2017) 131–134, https://doi.org/10.1016/j.algal.2017.07.012.
[85] J.M. Jarvis, N.M. Sudasinghe, K.O. Albrecht, A.J. Schmidt, R.T. Hallen, D. B. Anderson, J.M. Billing, T.M. Schaub, Impact of iron porphyrin complexes when hydroprocessing algal HTL biocrude, Fuel 182 (2016) 411–418, https://doi.org/10.1016/j.fuel.2016.05.107.
[86] K.K. Ramasamy, M.R. Thorson, J.M. Billing, J. Holladay, C. Drennan, B. Hoffman, Z. Haq, Hydrothermal Liquefaction : Path to Sustainable Aviation Fuel, 2021. https://www.osti.gov/biblio/1821809.
[87] M.S. Haider, M.A. Isik, D. Castello, L.A. Rosendahl, T.H. Pedersen, Demineralization of miscanthus biocrude obtained from catalytic hydrothermal liquefaction: Conditioning through acid washing, Processes 9 (2021) 1035, https://doi.org/10.3390/pr9061035.
[88] J.S. Ramírez-Pradilla, C. Blanco-Tirado, M. Hubert-Roux, P. Giusti, C. Afonso, M. Y. Combariza, Comprehensive Petroporphyrin Identification in Crude Oils Using Highly Selective Electron Transfer Reactions in MALDI-FTICR-MS, Energy Fuels 33 (2019) 3899–3907, https://doi.org/10.1021/acs.energyfuels.8b04325.
[89] B.E.O. Eboibi, D.M. Lewis, P.J. Ashman, S. Chinnasamy, Hydrothermal liquefaction of microalgae for biocrude production: Improving the biocrude properties with vacuum distillation, Bioresour. Technol. 174 (2014) 212–221, https://doi.org/10.1016/j.biortech.2014.10.029.
[90] J. Jiang, P.E. Savage, Using Solvents to Reduce the Metal Content in Crude Bio-oil from Hydrothermal Liquefaction of Microalgae, Ind. Eng. Chem. Res. 58 (2019) 22488–22496, https://doi.org/10.1021/acs.iecr.9b03497.
[91] Y. Tong, T. Yang, B. Li, X. Kai, R. Li, Two-stage liquefaction of sewage sludge in methanol-water mixed solvents with low-medium temperature, J. Supercrit. Fluids 168 (2021), 105094, https://doi.org/10.1016/j.supflu.2020.105094.
[92] D.R. Vardon, B.K. Sharma, J. Scott, G. Yu, Z. Wang, L. Schideman, Y. Zhang, T. J. Strathmann, Chemical properties of biocrude oil from the hydrothermal

liquefaction of Spirulina algae, swine manure, and digested anaerobic sludge, Bioresour. Technol. 102 (2011) 8295–8303, https://doi.org/10.1016/j.biortech.2011.06.041.
[93] D. Xu, Y. Wang, G. Lin, S. Guo, S. Wang, Z. Wu, Co-hydrothermal liquefaction of microalgae and sewage sludge in subcritical water: Ash effects on bio-oil production, Renew. Energy. 138 (2019) 1143–1151, https://doi.org/10.1016/j.renene.2019.02.020.
[94] S. Kandasamy, B. Zhang, Z. He, H. Chen, H. Feng, Q. Wang, B. Wang, N. Bhuvanendran, S. Esakkimuthu, V. Ashokkumar, M. Krishnamoorthi, Hydrothermal liquefaction of microalgae using Fe3O4 nanostructures as efficient catalyst for the production of bio-oil: Optimization of reaction parameters by response surface methodology, Biomass Bioenergy 131 (2019), 105417, https://doi.org/10.1016/j.biombioe.2019.105417.
[95] K. Malins, V. Kampars, J. Brinks, I. Neibolte, R. Murnieks, R. Kampare, Bio-oil from thermo-chemical hydro-liquefaction of wet sewage sludge, Bioresour. Technol. 187 (2015) 23–29, https://doi.org/10.1016/j.biortech.2015.03.093.
[96] Y. Chen, R. Mu, M. Yang, L. Fang, Y. Wu, K. Wu, Y. Liu, J. Gong, Catalytic hydrothermal liquefaction for bio-oil production over CNTs supported metal catalysts, Chem. Eng. Sci. 161 (2017) 299–307, https://doi.org/10.1016/j.ces.2016.12.010.
[97] F. Qian, X. Zhu, Y. Liu, Q. Shi, L. Wu, S. Zhang, J. Chen, Z.J. Ren, Influences of Temperature and Metal on Subcritical Hydrothermal Liquefaction of Hyperaccumulator: Implications for the Recycling of Hazardous Hyperaccumulators, Environ. Sci. Technol. 52 (2018) 2225–2234, https://doi.org/10.1021/acs.est.7b03756.
[98] X. Cao, X. Peng, S. Sun, L. Zhong, W. Chen, S. Wang, R.C. Sun, Hydrothermal conversion of xylose, glucose, and cellulose under the catalysis of transition metal sulfates, Carbohydr. Polym. 118 (2015) 44–51, https://doi.org/10.1016/j.carbpol.2014.10.069.
[99] E.Z. Hoşgün, One-pot hydrothermal conversion of poppy stalks over metal chloride catalysts, Biomass Convers. Biorefinery. 11 (6) (2021) 2703–2710.
[100] L. Kong, G. Li, H. Wang, W. He, F. Ling, Hydrothermal catalytic conversion of biomass for lactic acid production, J. Chem. Technol. Biotechnol. 83 (2008) 383–388, https://doi.org/10.1002/jctb.1797.
[101] J.H. Lee, H. Hwang, J.W. Choi, Effects of transition metals on hydrothermal liquefaction of empty fruit bunches (EFB) for conversion to biofuel and valuable chemicals, Energy. 162 (2018) 1–9, https://doi.org/10.1016/j.energy.2018.07.197.
[102] K. Kumar, F. Parveen, T. Patra, S. Upadhyayula, Hydrothermal conversion of glucose to levulinic acid using multifunctional ionic liquids: Effects of metal ion co-catalysts on the product yield, New J. Chem. 42 (2018) 228–236, https://doi.org/10.1039/c7nj03146g.
[103] S.M. Shahrul Nizan Shikh Zahari, N.A. Zulastry, H.H. Azman, A Preliminary Study of Catalytic Hydrothermal Conversion of Cellulose to Lactic Acid: Effects of Reaction Temperature and Metal Ion Catalyst, in, J. Phys. Conf. Ser. 1551 (1) (2020) 012014.
[104] X. Zhu, F. Qian, C. Zhou, L. Li, Q. Shi, S. Zhang, J. Chen, Inherent Metals of a Phytoremediation Plant Influence Its Recyclability by Hydrothermal Liquefaction, Environ. Sci. Technol. 53 (2019) 6580–6586, https://doi.org/10.1021/acs.est.9b00262.
[105] D.C. Elliott, P. Biller, A.B. Ross, A.J. Schmidt, S.B. Jones, Hydrothermal liquefaction of biomass: Developments from batch to continuous process, Bioresour. Technol. 178 (2015) 147–156, https://doi.org/10.1016/j.biortech.2014.09.132.
[106] Z.X. Xu, Y.Q. Shan, Z. Zhang, X.Q. Deng, Y. Yang, R. Luque, P.G. Duan, Hydrothermal carbonization of sewage sludge: Effect of inorganic salts on hydrochar's physicochemical properties, Green Chem. 22 (2020) 7010–7022, https://doi.org/10.1039/d0gc02615h.
[107] C. Liu, J. Xu, J. Hu, H. Zhang, R. Xiao, Metal Ion-Catalyzed Hydrothermal Liquefaction of Calcium Lignosulfonate in Subcritical Water, Chem. Eng. Technol. 40 (2017) 1092–1100, https://doi.org/10.1002/ceat.201600650.
[108] Z. Shen, F. Jin, Y. Zhang, B. Wu, A. Kishita, K. Tohji, H. Kishida, Effect of alkaline catalysts on hydrothermal conversion of glycerin into lactic acid, Ind. Eng. Chem. Res. 48 (2009) 8920–8925, https://doi.org/10.1021/ie900937d.
[109] J. Lu, J. Wu, L. Zhang, Z. Liu, Y. Wu, M. Yang, Catalytic hydrothermal liquefaction of microalgae over mesoporous silica-based materials with site-separated acids and bases, Fuel 279 (2020), 118529, https://doi.org/10.1016/j.fuel.2020.118529.
[110] S. Yin, A.K. Mehrotra, Z. Tan, Alkaline hydrothermal conversion of cellulose to bio-oil: Influence of alkalinity on reaction pathway change, Bioresour. Technol. 102 (2011) 6605–6610, https://doi.org/10.1016/j.biortech.2011.03.069.
[111] S. Yin, Z. Tan, Hydrothermal liquefaction of cellulose to bio-oil under acidic, neutral and alkaline conditions, Appl. Energy 92 (2012) 234–239, https://doi.org/10.1016/j.apenergy.2011.10.041.
[112] A. Galadima, O. Muraza, Hydrothermal liquefaction of algae and bio-oil upgrading into liquid fuels: Role of heterogeneous catalysts, Renew. Sustain. Energy Rev. 81 (2018) 1037–1048, https://doi.org/10.1016/j.rser.2017.07.034.
[113] W. Yang, X. Li, S. Liu, L. Feng, Direct hydrothermal liquefaction of undried macroalgae Enteromorpha prolifera using acid catalysts, Energy Convers. Manag. 87 (2014) 938–945, https://doi.org/10.1016/j.enconman.2014.08.004.
[114] Y.H. Xu, M.F. Li, Hydrothermal liquefaction of lignocellulose for value-added products: Mechanism, parameter and production application, Bioresour. Technol. 342 (2021), 126035, https://doi.org/10.1016/j.biortech.2021.126035.
[115] F. Cheng, G.A. Tompsett, C.M. Murphy, A.R. Maag, N. Carabillo, M. Bailey, J. J. Hemingway, C.I. Romo, A.D. Paulsen, P.E. Yelvington, M.T. Timko, Synergistic Effects of Inexpensive Mixed Metal Oxides for Catalytic Hydrothermal Liquefaction of Food Wastes, ACS Sustain. Chem. Eng. 8 (2020) 6877–6886, https://doi.org/10.1021/acssuschemeng.0c02059.
[116] A.A. Shah, S.S. Toor, F. Conti, A.H. Nielsen, L.A. Rosendahl, Hydrothermal liquefaction of high ash containing sewage sludge at sub and supercritical conditions, Biomass Bioenergy 135 (2020), 105504, https://doi.org/10.1016/j.biombioe.2020.105504.
[117] J. Lu, J. Zhang, Z. Zhu, Y. Zhang, Y. Zhao, R. Li, J. Watson, B. Li, Z. Liu, Simultaneous production of biocrude oil and recovery of nutrients and metals from human feces via hydrothermal liquefaction, Energy Convers. Manage. 134 (2017) 340–346, https://doi.org/10.1016/j.enconman.2016.12.052.
[118] J. Watson, T. Wang, B. Si, W.T. Chen, A. Aierzhati, Y. Zhang, Valorization of hydrothermal liquefaction aqueous phase: pathways towards commercial viability, Prog. Energy Combust. Sci. 77 (2020), 100819, https://doi.org/10.1016/j.pecs.2019.100819.
[119] P. Biller, I. Johannsen, J.S. dos Passos, L.D.M. Ottosen, Primary sewage sludge filtration using biomass filter aids and subsequent hydrothermal co-liquefaction, Water Res. 130 (2018) 58–68, https://doi.org/10.1016/j.watres.2017.11.048.
[120] R. Posmanik, R.A. Labatut, A.H. Kim, J.G. Usack, J.W. Tester, L.T. Angenent, Coupling hydrothermal liquefaction and anaerobic digestion for energy valorization from model biomass feedstocks, Bioresour. Technol. 233 (2017) 134–143, https://doi.org/10.1016/j.biortech.2017.02.095.
[121] S. Hao, S. Ren, N. Zhou, H. Chen, M. Usman, C. He, Q. Shi, G. Luo, S. Zhang, Molecular composition of hydrothermal liquefaction wastewater from sewage sludge and its transformation during anaerobic digestion, J. Hazard. Mater. 383 (2020), 121163, https://doi.org/10.1016/j.jhazmat.2019.121163.
[122] M. Usman, S. Hao, H. Chen, S. Ren, D.C.W. Tsang, S. O-Thong, G. Luo, S. Zhang, Molecular and microbial insights towards understanding the anaerobic digestion of the wastewater from hydrothermal liquefaction of sewage sludge facilitated by granular activated carbon (GAC), Environ. Int. 133 (2019) 105257.
[123] P. Wang, Y. Sakhno, S. Adhikari, H. Peng, D. Jaisi, T. Soneye, B. Higgins, Q. Wang, Effect of ammonia removal and biochar detoxification on anaerobic digestion of aqueous phase from municipal sludge hydrothermal liquefaction, Bioresour. Technol. 326 (2021), 124730, https://doi.org/10.1016/j.biortech.2021.124730.
[124] F. Conti, S.S. Toor, T.H. Pedersen, T.H. Seehar, A.H. Nielsen, L.A. Rosendahl, Valorization of animal and human wastes through hydrothermal liquefaction for biocrude production and simultaneous recovery of nutrients, Energy Convers. Manag. 216 (2020), 112925, https://doi.org/10.1016/j.enconman.2020.112925.
[125] J. Lu, J. Watson, J. Zeng, H. Li, Z. Zhu, M. Wang, Y. Zhang, Z. Liu, Biocrude production and heavy metal migration during hydrothermal liquefaction of swine manure, Process Saf. Environ. Prot. 115 (2018) 108–115, https://doi.org/10.1016/j.psep.2017.11.001.
[126] H. Li, J. Lu, Y. Zhang, Z. Liu, Hydrothermal liquefaction of typical livestock manures in China: Biocrude oil production and migration of heavy metals, J. Anal. Appl. Pyrol. 135 (2018) 133–140, https://doi.org/10.1016/j.jaap.2018.09.010.
[127] J. Lu, J. Watson, Z. Liu, Y. Wu, Elemental migration and transformation during hydrothermal liquefaction of biomass, J. Hazard. Mater. 423 (2022), 126961, https://doi.org/10.1016/j.jhazmat.2021.126961.
[128] A.A. Carbonell-Barrachina, A. Jugsujinda, F. Burlo, R.D. Delaune, W.H. Patrick, Arsenic chemistry in municipal sewage sludge as affected by redox potential and pH, Water Res. 34 (1) (2000) 216–224.